nature communications

Article

https://doi.org/10.1038/s41467-025-58115-8

A combined adjuvant and ferritin nanocage based mucosal vaccine against *Streptococcus pneumoniae* induces protective immune responses in a murine model

Received: 4 June 2024

Accepted: 13 March 2025

Published online: 24 March 2025

Check for updates

Tien Duc Nguyen[1,2], Hoang Duy Le[1,2], Giang Chau Dang[1,2], Hyun Seok Jung[2], Yoonjoo Choi[2], Koemchhoy Khim[1,2], Young Kim[3], Shee Eun Lee[1,4,5] ✉ & Joon Haeng Rhee[1,2,6] ✉

Protein nanocages are multimeric structures that can be engineered to mimic the molecular conformation of microorganisms. Based on previous findings showing that a mucosal FlaB-tPspA fusion (flagellin fused with truncated PspA antigen of *Streptococcus pneumoniae*) vaccine-induced protective immune response against *S. pneumoniae*, we develop a ferritin nanocage vaccine displaying multivalent presentation of both antigen and adjuvant on a nanocarrier using the SpyTag/SpyCatcher strategy. The 1:1 antigen/adjuvant nanocage is further used as a mucosal vaccine, which can translocate to draining lymph nodes with higher efficiency than fusion vaccine. Moreover, intranasal immunization with the nanocage vaccine significantly enhances mucosal immune responses with more efficient B-cell memory generation and antibody maturation, as well as more balanced (Th1/Th2) immune responses with increased IFN-γ and IL-17 production, comparing with fusion vaccine. Mice immunized with the nanocage vaccine exhibited enhanced protection against lethal infection compare to the FlaB-tPspA fusion group. Our study thus demonstrates the effectiveness of an all-in-one nanocage mucosal vaccine platform, which guarantees enhanced protection with balanced immune responses.

The mucosae lining the respiratory, gastrointestinal, and genitourinary tracts serve as entry portals for foreign agents, including microbial pathogens. Mucosal vaccines have the potential to elicit more effective protective immune responses against pathogens at infection sites than parenteral vaccines through secretory IgA and cell-mediated immunity. Despite the advantages of mucosal vaccination, only a limited number of licensed mucosal vaccines are available. Licensed mucosal vaccines consist of live attenuated or inactivated whole-cell preparations, and no subunit mucosal vaccine has been approved yet[1,2]. Considering that licensed mucosal vaccines intrinsically contain pathogen-associated molecular patterns (PAMPs) as built-in adjuvants and the pathogen's cell bodies as the delivery system, whole-cell mimicking

[1]Clinical Vaccine R&D Center, Chonnam National University, Hwasun-gun, Jeonnam, Republic of Korea. [2]Combinatorial Tumor Immunotherapy MRC, Chonnam National University Medical School, Hwasun-gun, Jeonnam, Republic of Korea. [3]Department of Oral Pathology, Chonnam National University School of Dentistry, Gwangju, Republic of Korea. [4]National Immunotherapy Innovation Center, Hwasun-gun, Jeonnam, Republic of Korea. [5]Department of Pharmacology and Dental Therapeutics, Chonnam National University School of Dentistry, Gwangju, Republic of Korea. [6]Department of Microbiology, Chonnam National University Medical School, Hwasun-gun, Jeonnam, Republic of Korea. ✉e-mail: selee@chonnam.ac.kr; jhrhee@chonnam.ac.kr

subunit vaccine delivery units consisting of both adjuvant and protective antigens would overcome the safety concerns associated with whole-cell mucosal vaccines.

Protein nanocages are cage-like multimeric nanoscale structures composed of bio-degradable protein subunits. They serve as intracellular storage containers, provide structural support for assembling enzyme complexes, encapsulate genetic materials, and act as vehicles for transporting molecules within cells[3]. Given that several protein nanocages have been explored as potential carriers in biomedicine[4,5], they may help the development of whole-cell-mimicking vaccine delivery systems and/or mucosal vaccine formulations. Ferritin is a highly stable iron-storage protein found in humans and many other organisms and plays a crucial role in regulating iron homeostasis. Featuring a spherical structure mimicking virus particles composed of 24 subunits that self-assemble into hollow nanocages[6], ferritin has shown wide-range applications as a vaccine platform in preclinical and clinical settings[7–11].

Flagellin plays a dual role in biology; it functions as the structural foundation for the flagellar filaments in motile bacteria[12] while also serving as a cognate ligand for host pattern recognition receptors (PRRs), specifically Toll-like receptor 5 (TLR5) on the cell surface and the NAIP5/NLRC4 inflammasome in the cytosol[13–15]. Moreover, flagellin is a stable, self-assembling protein that retains its function even after various physicochemical challenges[16,17]. Based on these advantages, which include biochemical stability and activation of two different PAMP pathways, flagellin has been actively developed as a vaccine adjuvant and immunotherapeutic agent[18]. We have reported that the bacterial flagellin, *Vibrio vulnificus* FlaB, is a versatile adjuvant suitable for a broad spectrum of mucosal vaccines and immunotherapies[19–23]. Given that flagellin is a protein-based PAMP, FlaB could facilely be engineered as a built-in adjuvant using recombinant DNA technology. Its inherent stability and high expression propensity make it an excellent fusion partner for difficult-to-express antigens. Our previous studies showed that flagellin fusion protein vaccines induce strongly enhanced antigen-specific immune responses, producing excellent protective or therapeutic outcomes[23–25].

A stable bioconjugation process should be employed to develop multi-component protein nanocage complexes consisting of molecularly defined vaccine antigens and protein-based adjuvants in a single-unit structure. SpyTag and SpyCatcher spontaneously form isopeptide bonds for reconstitution over an extensive temperature range (4–37 °C), in the pH range of 5–8, and under diverse buffer conditions, thereby enabling specific covalent coupling of proteins[26–29]. Following the development of the bacteria-derived spontaneously ligating SpyTag-SpyCatcher system in 2012, endeavors were focused on optimizing this linkage system to enhance its efficacy and stability[28,30,31]. These efforts enabled efficient macromolecular assembly[32] and offered the freedom to design complex protein structures, including multivalent vaccines, in a plug-and-play fashion[33]. Moreover, studies for HBV[34] and HIV[35] vaccines employing SpyTag-SpyCatcher for antigen conjugation to a nanoparticle scaffold have demonstrated enhanced immunogenicity compared to their unlinked monomeric counterparts.

Streptococcus pneumoniae is the leading cause of bacterial pneumonia worldwide, especially in children[36]. It causes 1.2 million deaths every year, and children in developing countries are the most vulnerable individuals[1]. Antibodies against capsular polysaccharides have proven protective, and prophylactic vaccines have been developed against prevalent capsular serotypes[37,38]. The polysaccharide vaccine can stimulate protective humoral immunity in immune-competent subjects but weakly induces cellular immunity and durable immune memory, making the vaccine less effective in high-risk groups such as children, elderly populations, and immunocompromised individuals[39–41]. Despite their well-proven benefits, pneumococcal conjugate vaccines (PCV) have limitations, such as limited coverage against clinical strains and serving the selective pressure that leads to new serotypes[42,43]. To address these concerns, efforts have been made to develop new types of pneumococcal vaccines[44,45]. Among them, subunit vaccines against *S. pneumoniae* proteins contributing to pathogenesis have been actively studied. One of those promising protein vaccine targets is pneumococcal surface protein A (PspA)[24,46]. In nasopharyngeal carriage and infectious invasion, PspA plays a crucial role in preventing the attachment of complement components on the bacterial surface, thus inhibiting the opsonization and killing of *S. pneumoniae*. Vaccination with PspA induces anti-PspA antibodies against many pneumococcal strains, protecting mice from lethal *S. pneumoniae* infections[47,48]. Our previous study showed that the FlaB-tPspA (truncated fragment of extracellular PspA) fusion protein could induce a more robust immune response than a simple mixture of tPspA and FlaB[24]. However, although the FlaB-tPspA fusion protein induced excellent protective antibody responses, it could not induce notable cellular immunity, which may contribute to more effective eradication of infection/colonization and longer immune memory.

In this study, we develop the FPB NC, a ferritin-based nanocage vaccine concomitantly displaying both the tPspA antigen and FlaB mucosal adjuvant, using the SpyTag-SpyCatcher technology. The built-in adjuvanted ferritin nanocage mucosal vaccine against *S. pneumoniae* induce high-quality protective immune responses. We thus propose a nanocarrier vaccine platform that could be applied to developing mucosal vaccines against multitudinous pathogens.

Results

Development of a ferritin-based nanocage vaccine consisting of tPspA antigen and FlaB adjuvant (FPB) using the SpyTag-SpyCatcher system

To develop a nanocage vaccine targeting *S. pneumoniae*, we harnessed the SpyTag/SpyCatcher system into a ferritin nanocage scaffold[29,31] (Fig. 1A and Supplementary Movie 1). In the present study, we selected the ferritin gene of *Pyrococcus furios* (Pf-ferritin, referred to as ferritin or Ftn hereafter), which was previously utilized for HIV-1 vaccine development[49,50]. First, we generated the recombinant SpyTag-Ftn nanocage scaffold, SpyCatcher-tPspA antigen, and SpyCatcher-FlaB adjuvant (Fig. 1A, B). Size exclusion chromatography was also employed to attain the SpyTag-Ftn protein's high purity. The above three components were co-incubated overnight at 4 °C at varying molar ratios for vaccine nanocage assembly. Each element in the assembled nanocages was confirmed by SDS-PAGE (Fig. S1A). Covalent conjugation of SpyTag-SpyCatcher led to the appearance of two new bands, at 62.3 kDa and 76.1 kDa, corresponding to Ftn-ST-SC-tPspA and Ftn-ST-SC-FlaB, respectively (Figs. S1A and 1B).

Subsequently, the Ftn-tPspA-FlaB nanocage (FPB NCs) was further purified via ion exchange chromatography (Fig. 1B). SDS-PAGE confirmed the purity of the FPB NCs. When the nanocage (NC) contained a more significant proportion of the tPspA antigen, the Ftn-ST-SC-tPspA band intensity increased. In contrast, when the flagellin adjuvant (FlaB) was predominant, the Ftn-ST-SC-FlaB band was the most prominent (Fig. S1B). This result suggested that changing each component's concentration could tractably modulate the antigen and flagellin adjuvant ratio. To identify the most suitable nanocage candidates for preserving the biological functionality of FlaB, we conducted a TLR5-dependent NFκB reporter assay utilizing an equivalent amount of FlaB as the control. The results demonstrated that compared with FlaB, FPB NC (24:10:10 in molar ratio), FPB NC (24:05:15), and FPB NC (24:6.7:13) displayed comparably enhanced TLR5 stimulation activity than FlaB. It was observed that FPB NC (24:13.3:6.7) exhibited significantly reduced NFκB activation, while the other ratios showed no notable differences (Fig. S1C). Considering these findings and our previous study results[24], we selected FPB NC (24:10:10), characterized by an optimal antigen/adjuvant ratio and robust TLR5 stimulation activity, for further studies.

https://doi.org/10.1038/s41467-025-58115-8

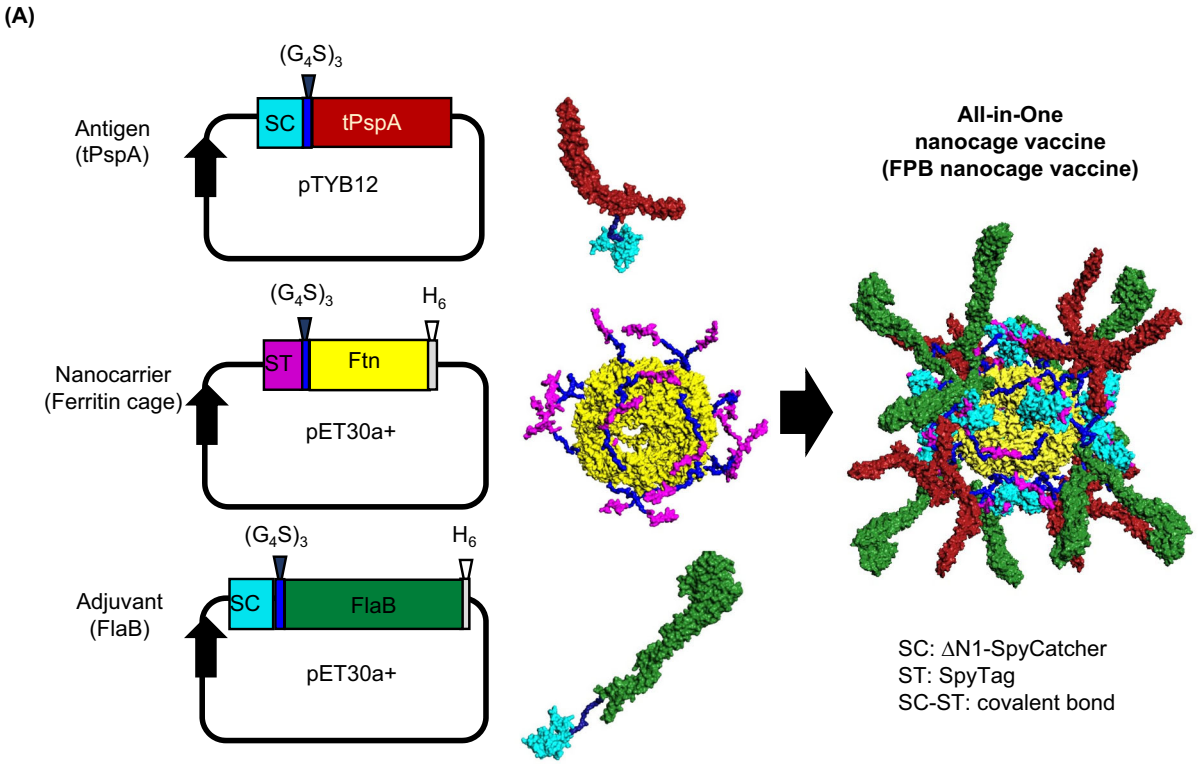

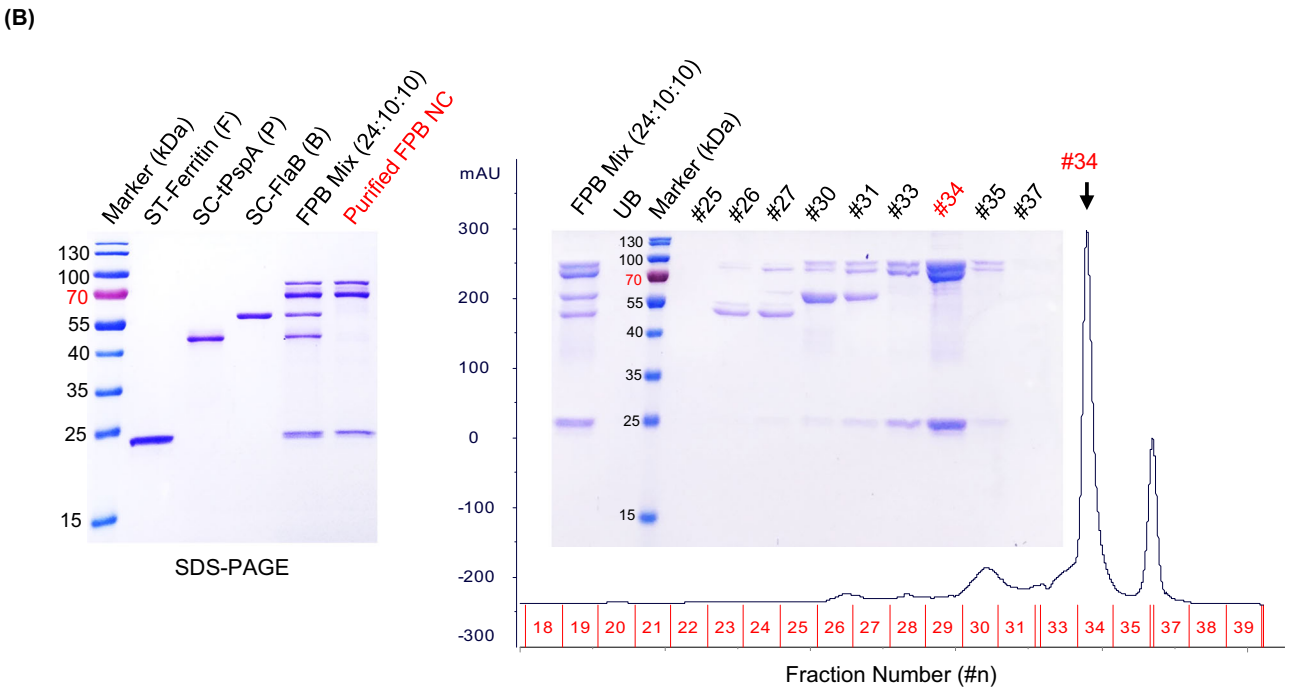

Fig. 1 | Development of a ferritin-based nanocage vaccine consisting of the tPspA antigen and FlaB adjuvant (Ftn-tPspA-FlaB nanocage: FPB NC) using the SpyTag-SpyCatcher system. A Schematic representation of the strategy for developing the FPB nanocage vaccine. This diagram provides a visual representation of the plasmid constructs. It simulates the protein structure of the critical components of the ferritin-tPspA-FlaB nanocage (FPB NC): SpyTag-ferritin, SpyCatcher-tPspA, and SpyCatcher-FlaB. The depicted DNA fragments correspond to essential elements of the constructs representing ΔN1-SpyCatcher (SC, cyan), SpyTag (ST, violet), truncated PspA (tPspA; amino acid 3-236, red), FlaB (green), and ferritin (yellow). SC-tPspA, ST-Ftn, and SC-FlaB each contain a $(G_4S)_3$ linker (dark blue). The resulting FPB nanocage structure was simulated in three dimensions. **B** Sodium dodecyl sulfate-polyacrylamide gel electrophoresis (SDS-PAGE) analysis. Recombinant proteins, including ST-Ftn, SC-tPspA, SC-FlaB, the FPB mixture (24:10:10), and purified FPB NC by ion-exchange chromatography (Left panel) were resolved using SDS-PAGE. The right panel presents a representative ion exchange chromatogram alongside the corresponding SDS-PAGE pattern. Data are a representative of three independent experiments.

https://doi.org/10.1038/s41467-025-58115-8

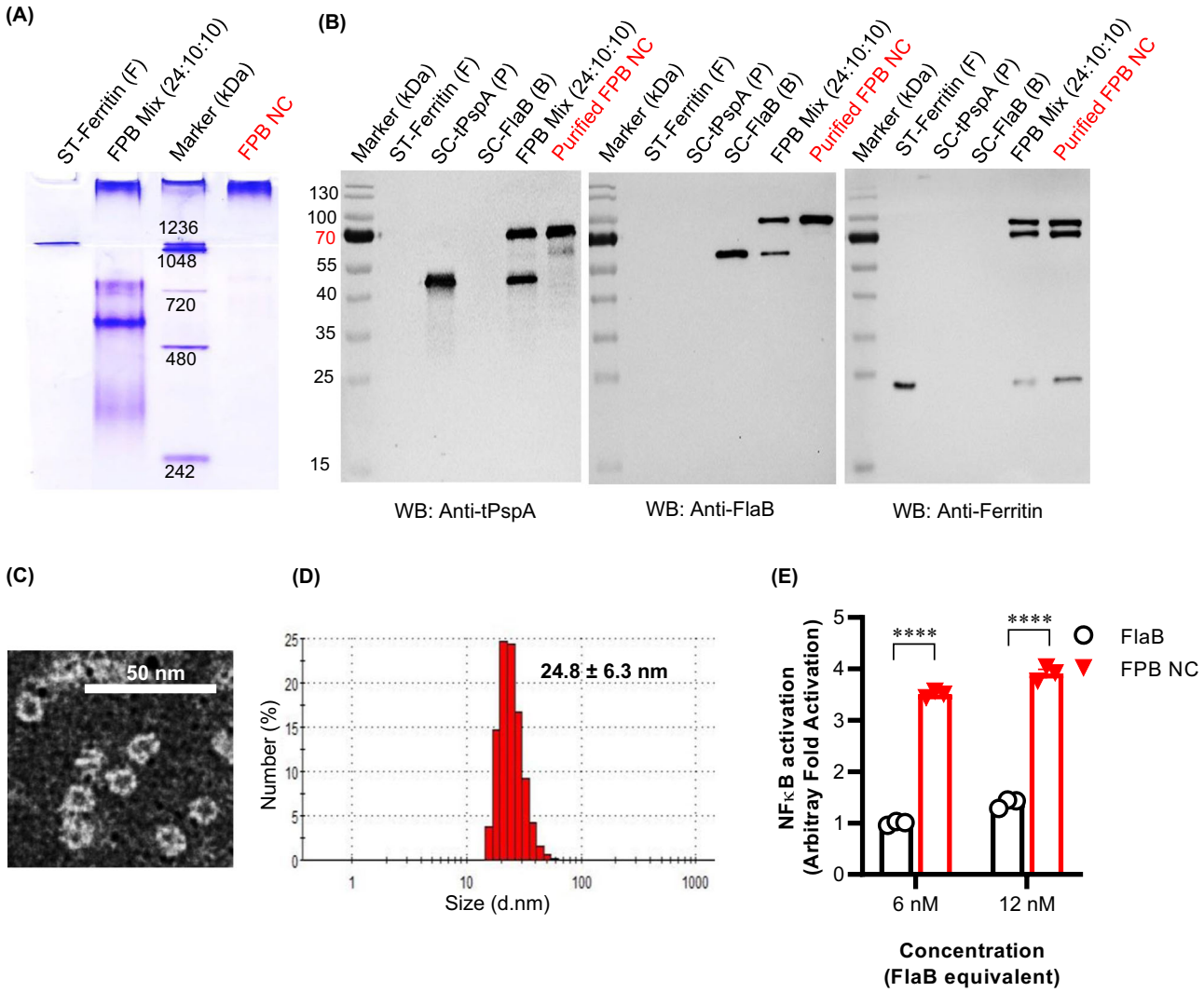

Fig. 2 | Characteristics of the FPB NC vaccine. A Native-PAGE analysis of FPB NC. The Ftn-tPspA-FlaB nanocage mixture was incubated for 16 h at 4 °C, or the FPB NC purified by ion-exchange chromatography was mixed with native loading buffer and loaded onto a 10% native-PAGE gel. A purified ST-Ftn nanocage (ST-Ftn NC) was used as a control. **B** Western blot of FPB NC. The recombinant proteins were resolved using SDS-PAGE, and subsequently, the protein bands were detected and visualized using the anti-tPspA, anti-FlaB, or anti-Ftn antibody. **C** TEM image of the FPB NC. The purified FPB NCs were negatively stained with phosphotungstic acid (scale bar = 50 nm). **D** Dynamic light scattering (DLS)-mediated size measurement of FPB NC. The data revealed that FPB NC has an average diameter of 24.8 ± 6.3 nm. **E** Determination of TLR5-dependent NFκB stimulation activity of FPB NC. The relative luciferase activity levels in the cell extracts were analyzed by a dual-luciferase reporter assay system and normalized using the pCMV-β-galactosidase plasmid as a control. The same molar ratios of proteins (FlaB equivalent) were used, and PBS was used as a negative control ($n = 3$ biological replicates). Data are presented as mean values ± SEM. Statistical differences were analyzed using Student's t test. ** $P < 0.01$; *** $P < 0.001$; **** $P < 0.0001$. Source data are provided as a Source Data file. Detail P values are provided in the Source Data file.

Characterization of the ferritin-tPspA-FlaB nanocage (FPB NC) vaccine

We performed the native-gel electrophoresis to confirm FPB NC's successful assembly further. FPB NC was observed to be confined within the stacking gel, whereas ST-Ftn was located between the stacking and resolving gels. This finding implied that the FPB NC was stably formed and possessed a considerably bigger physical mass than the ST-Ftn core (Fig. 2A). Notably, FPB Mix (24:10:10) and pre-formed FPB NC did not show any ST-Ftn NC bands on the native gel. This result suggested that tPspA or FlaB bound all of the ferritin core, and free ST-Ftn bands on the FPB NC SDS-PAGE gel likely might have originated from some SpyTags captured inside the nanocage or from a minor unconjugated fraction incorporated into the nanocage structure along with the majority of SpyCatcher conjugated components. The correct assembly of the nanocage was further validated through western blot analysis (Fig. 2B). The anti-tPspA antibody (Ab) identified SC-tPspA (band at 38.5 kDa) and Ftn-ST-SC-tPspA (band at 62.3 kDa), confirming the proper antigenic presentation of tPspA on the nanocage. Similarly, the anti-FlaB Ab recognized SC-FlaB (band at 52.3 kDa) and Ftn-ST-SC-FlaB (band at 76.1 kDa). Additionally, the anti-Ftn Ab detected ST-Ftn, Ftn-ST-SC-tPspA, and Ftn-ST-SC-FlaB, confirming the appropriate structural arrangement of ferritins for their self-assembly into the nanocage. These collective findings provide physical solid evidence for the integrity of the nanocage vaccine, which will present proper antigenicity and adjuvanticity to both tPspA and FlaB, respectively.

Further characterization of FPB NC was carried out using transmission electron microscopy (TEM) and the dynamic light scattering (DLS) analyzer to assess its homogeneity and size. TEM revealed that FPB NCs exhibited well-defined and uniformly spherical nanocage structures (Fig. 2C). The average size of FPB NC was 24.8 ± 6.3 nm (Fig. 2D). In comparison, the ST-Ftn core, which forms 24-mer nanocages, was 2.1-fold smaller than FPB NC, with an average diameter of 11.8 ± 2.3 nm (Fig. S2). To evaluate the in vitro functionality of the purified nanocage, we compared its TLR5 stimulation activity with that

https://doi.org/10.1038/s41467-025-58115-8

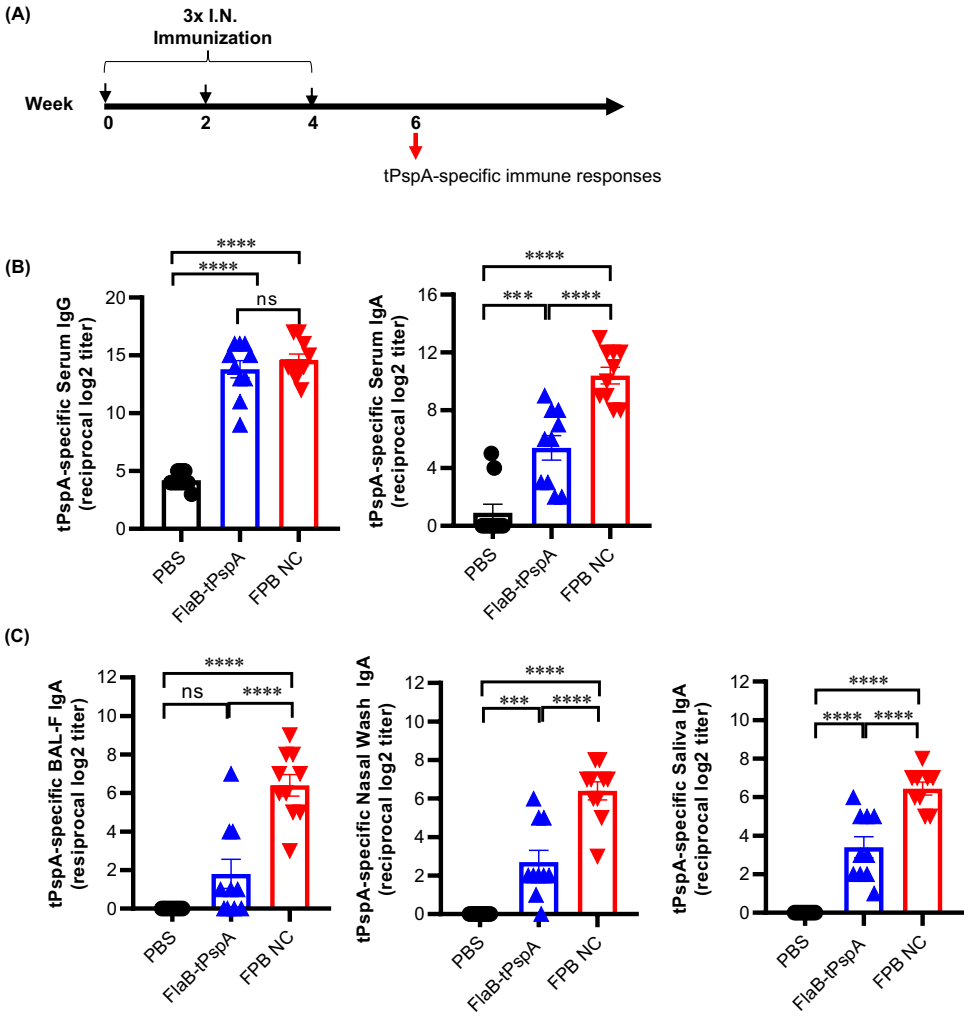

Fig. 3 | Antigen-specific systemic and mucosal antibody responses induced by intranasal (I.N.) immunization of the FPB NC vaccine. A Experimental schedule for immunization. BALB/c mice were intranasally (I.N.) immunized with either phosphate-buffered saline (PBS), 6.5 μg of FlaB-tPspA, or 14.5 μg of FPB NC three times at two-week intervals for a total volume of 20 μl per mouse. **B** Determination of tPspA-specific systemic IgG or IgA titers. Two weeks after the final immunization, the levels of tPspA-specific serum IgG were evaluated using the enzyme-linked immunosorbent assay (ELISA). **C** Determination of the tPspA-specific mucosal IgA titer. Two weeks after the final immunization, tPspA-specific serum IgA levels in BAL-F, nasal wash, or saliva were evaluated using ELISA ($n = 10$ biological replicates). Data are presented as mean values ± SEM. Statistical differences were analyzed using one-way ANOVA. Statistical significance: $^{*}P < 0.05$; $^{**}P < 0.01$; $^{***}P < 0.001$; $^{****}P < 0.0001$; ns = not significant. Source data are provided as a Source Data file. Detail *P* values are provided in the Source Data file.

of free FlaB at two stoichiometric concentrations (6 and 12 nM) while maintaining the same molar ratio of FlaB in FPB NC. Compared with free FlaB, FPB NC demonstrated a 3.50-fold and 2.82-fold enhancement in NFκB activation at concentrations of 6 nM and 12 nM, respectively (Fig. 2E). This implies that the FPB NC exposes more TLR5-binding domains of FlaB on its surface compared to free FlaB, where such domains are obscured by the axial assembly of monomers[13,14]. The simultaneous conjugation of tPspA to the ferritin core along with FlaB might have prevented the hiding of TLR5-binding domains by homologous FlaB polymerization, as predicted by computational structure simulation (Fig. 1A and Supplementary Movie 1). By employing the 'SpyTag/SpyCatcher click model', we successfully displayed a functional FlaB adjuvant and tPspA antigen on the surface of a ferritin core nanocage.

Intranasal immunization of FPB NC induced more robust mucosal immune responses than immunization with FlaB-tPspA

Our previous study reported that intranasally (I.N.) administered FlaB-tPspA fusion protein induced more potent antibody responses in mucosal and systemic immune compartments than in a mixture of FlaB and tPspA[24]. In this context, we speculated that FPB NC should induce more robust immune responses against tPspA than the FlaB-tPspA since the FPB nanocages induce more robust TLR5 activation and can present antigens in multivalency (Figs. 3C, 1A and Supplementary Movie 1). To compare the tPspA-specific antibody responses elicited by FPB NC and the FlaB-tPspA fusion protein, BALB/c mice were subjected to I.N. immunization with three different formulations: PBS alone, 6.5 μg of FlaB-tPspA, or 14.5 μg of FPB NC. Two weeks after the final vaccination, we collected serum, nasal wash, bronchoalveolar lavage fluid (BAL-F), and saliva to assess tPspA-specific antibody titers using the enzyme-linked immunosorbent assay (ELISA) (Fig. 3A). As shown in Fig. 3B, both the FlaB-tPspA (13.8 ± 0.742 Log_2)- and FPB NC (14.6 ± 0.521 Log_2)-immunized groups exhibited similar tPspA-specific serum IgG titers (ns $P > 0.05$ for FlaB-tPspA vs. FPB NC). Nonetheless, compared with FlaB-tPspA (5.4 ± 0.846 Log_2) vaccination, FPB NC immunization (10.4 ± 0.581 Log_2) resulted in more vital anti-tPspA serum IgA responses (**** $P < 0.0001$; Fig. 3B). These results suggest that FPB NC may induce a more robust IgA class switching, while IgG responses are comparably activated by FPB NC and FlaB-tPspA. More notably, the mice immunized with FPB NC (BAL-F 6.4 ± 0.562; nasal

wash 6.4 ± 0.476; saliva 6.4 ± 0.338 Log_2) exhibited significantly enhanced secretory IgA (sIgA) responses in BAL-F, nasal wash, and saliva compared to FlaB-tPspA (BAL-F 1.8 ± 0.757; nasal wash 2.7 ± 0.616; saliva 3.4 ± 0.542 Log_2) (**** $P < 0.0001$; Fig. 3C). Collectively, these results indicate that I.N. immunization with the FPB NC vaccine more potently stimulated sIgA responses than immunization with the tPspA-FlaB fusion vaccine. This result led us to hypothesize that the antibody responses induced by the two vaccines employ distinctive immune activation processes.

The FPB NC vaccine induces more efficient B-cell differentiation and antibody maturation than FlaB-tPspA

Acquiring durable immunity through the induction of long-lived plasma cells and memory B cells is one of the critical goals of prophylactic vaccines[51]. To determine why the FPB NC was superior to FlaB-tPspA, we examined long-lived plasma cells in the bone marrow and memory B cells in the spleen using the ELISPOT assay. A significantly greater number of IgA-producing plasma cells (*$P < 0.05$ for FlaB-tPspA vs. FPB NC; Fig. 4A) and memory B cells (**$P < 0.01$ for FlaB-tPspA vs. FPB NC; Fig. 4B) were observed in FPB NC (12.25 ± 2.839 IgA-producing plasma cell/10^6 bone marrow cells; 13.5 ± 2.901 memory B cell/10^6 splenocytes)-immunized mice than in FlaB-tPspA (3.5 ± 0.645 IgA-producing plasma cell/10^6 bone marrow cells; 1.0 ± 0.707 memory B cell/10^6 splenocytes)-immunized mice. This result is consistent with systemic and secretory IgA production patterns in serum and mucosal secretions (Fig. 3B, C). These findings highlight the superior capacity of the FPB NC group for inducing long-lasting memory B cells and plasma cells producing IgA antibodies.

Furthermore, to assess qualitative differences in antibody responses between the FPB NC and FlaB-tPspA vaccines, we carried out a modified ELISA that could evaluate the avidity of tPspA-specific antibodies as previously reported[52,53]. As shown in Fig. 4C, after the second immunization, FPB NC immunization was superior in inducing higher avidity of tPspA-specific serum IgG (avidity index, 0.500 ± 0.023) than was FlaB-tPspA immunization (avidity index, 0.235 ± 0.066) (**$P < 0.01$ for FlaB-tPspA vs. FPB NC). Notably, no significant differences were observed after the third immunization, implying that antibody maturation had plateaued. These results strongly indicate that the nanocage vaccine facilitates more efficient B-cell differentiation and antibody maturation than the fusion protein vaccine. It was previously suggested that nanoscale-sized molecules within the 10 to 200 nm range exhibit increased delivery efficiency to lymph nodes (LNs)[3]. We speculated that related characteristics of FPB NC may have contributed to the above-mentioned potentiated IgA responses.

The FPB NC vaccine induces balanced immune responses

To evaluate the Th1/Th2 immune balance induced by FPB NC immunization compared to that in the FlaB-tPspA group, we measured the ratio of tPspA-specific IgG_{2a}/IgG_1 in the antisera. The results revealed a statistically significant difference, with the tPspA-specific IgG_{2a}/IgG_1 ratio significantly higher in the FPB NC-immunized group (0.925 ± 0.045) compared to the FlaB-tPspA group (0.581 ± 0.084) (**$P < 0.01$; Fig. 4D). The higher IgG2a/IgG1 ratio observed in the FPB NC vaccine group than that of the FlaB-tPspA group suggests that the FPB NC vaccine would be more effective in inducing cell-mediated immune responses. In this context, tPspA-specific production of IFN-γ, IL-4, and IL-17 was assessed in splenocytes. As shown in Fig. 4E, FPB NC-vaccinated mice exhibited significantly increased IFN-γ (7.56 ± 0.841 ng/ml) and IL-17 (1932.8 ± 198.15 pg/ml) production compared with FlaB-tPspA-immunized mice (3.69 ± 0.631 ng/ml IFN-γ and 584.4 ± 214.18 pg/ml IL-17) (FlaB-tPspA vs. FPB NC; IFN-γ, *$P < 0.05$ and IL-17, **$P < 0.01$). In contrast, no significant difference was observed in IL-4 levels. These findings indicate that the nanocage mucosal vaccine should be more efficacious in activating antigen-specific Th1 and Th17 responses than the protein hybrid vaccine.

Nanocages enhance the delivery of antigens and flagellin adjuvants to the draining lymph nodes

To induce effective antibody responses, after reaching the draining LNs, antigens should encounter B cells in the germinal center (GC) and receive sufficient help from follicular helper T cells (Tfhs) and follicular dendritic cells (FDCs). GC B-Tfh-FDC interactions are crucial for isotype switching, affinity maturation, and memory generation[54]. In light of these principles, we tracked the distribution of FPB NC in LNs after in vivo administration. The FPB NC and FlaB-tPspA were conjugated with the FNR675 dye and injected by subcutaneous (S.C.) administration in the groin. As shown in Fig. 5A, distinct patterns of antigen distribution between FPB NC and FlaB-tPspA were observed under confocal microscopy three hours post-administration. In animals vaccinated with FPB NC, a higher frequency of red fluorescence, corresponding to FNR675-conjugated FPB NC, was noted compared with those administered with FlaB-tPspA in the draining LNs.

More $CD11c^+$ dendritic cells were also recruited to the FPB NC drainage location, suggesting that more robust antigen presentation may have contributed to the enhanced efficacy in humoral and cellular immune responses (Fig. 5A). When the same amount was administered, a higher number of $CD11c^+$ cells were observed in the draining LNs (2.202 ± 0.087%, FPB NC and 1.582 ± 0.151%, FlaB-tPspA). (Fig. 5B, C upper panel, **$P < 0.01$), and higher FNR675 signals were associated with $CD11c^+$ cells (Fig. 5B, C lower, panel, *$P < 0.05$) in FPB NC (1.374 ± 0.24%) administered mice than those administered with FlaB-tPspA (0.622 ± 0.11%). Of note, FPB NCs appeared to expand and actively interact with $CD169^+$ subcapsular sinus macrophages (Fig. 5A). The subcapsular macrophage layer was significantly thicker in FPB NC immunized LNs than that of FlaB-tPspA immunized LNs (Fig. 5A). In the thickened subcapsular macrophage layer, FPB NC was closely associated with macrophage cells.

To assess FlaB adjuvant's involvement in interacting with $CD169^+$ subcapsular sinus macrophages, we developed ferritin nanocages presenting FlaB adjuvant (Ftn:FlaB:FB NC) (Fig. S2C, S2E) solely and ferritin nanocages displaying only tPspA antigen (Ftn:tPspA; FP NC) (Fig. S2D, S2E). And both nanocages were conjugated with FNR675. Subsequently, these conjugated proteins were subcutaneously injected into BALB/c mice, and inguinal lymph nodes (iLNs) were harvested after 3 h for FACS analysis to examine NCs' colocalization with $CD169^+$ cells. A significantly higher FNR675 signal associated with $CD169^+$ cells in draining LNs was also noted in FPB NC (3.76 ± 0.499%) and FB NC (3.06 ± 0.324%)-administered mice than Ftn NC group (0.623 ± 0.123%) or FP NC (1.147 ± 0.253%). These results suggest a significant role for FlaB in the association of nanocages with $CD169^+$ subcapsular sinus macrophages (Fig. S3A, S3B). It is known that nanoparticles can readily gain access to lymphatics and are drained directly to LN sinuses, including both the subcapsular and medullary sinuses, within minutes[34,55]. Subcapsular sinus macrophages have poor internalization and degradation capabilities and play an essential role in acquiring and transferring particulate antigens to B cells[56]. More striking was that B cell areas were extensively expanded after the FPB NC administration even as early as 3 h, while FlaB-tPspA administration did not (Fig. 5A). This noteworthy result strongly suggested that the efficient delivery of nanocage molecules to the lymph nodes and facilitated translocation to the B-cell area, presumably piggybacked by subcapsular sinus macrophages, contributed to the induction of a more robust B-cell expansion and differentiation.

FPB NC prompts GC formation and rapidly expands Tfhs

The GC plays a crucial role in the humoral immune response by facilitating the generation of high-affinity antibodies, isotype class switching, and long-lived memory B cells. To assess the GC formation, we performed I.N. administration of FPB NC and FlaB-tPspA two times at 1-week intervals. The cLNs were collected one week after the last immunization, and the isolated fresh LNs were observed for GCs after

https://doi.org/10.1038/s41467-025-58115-8

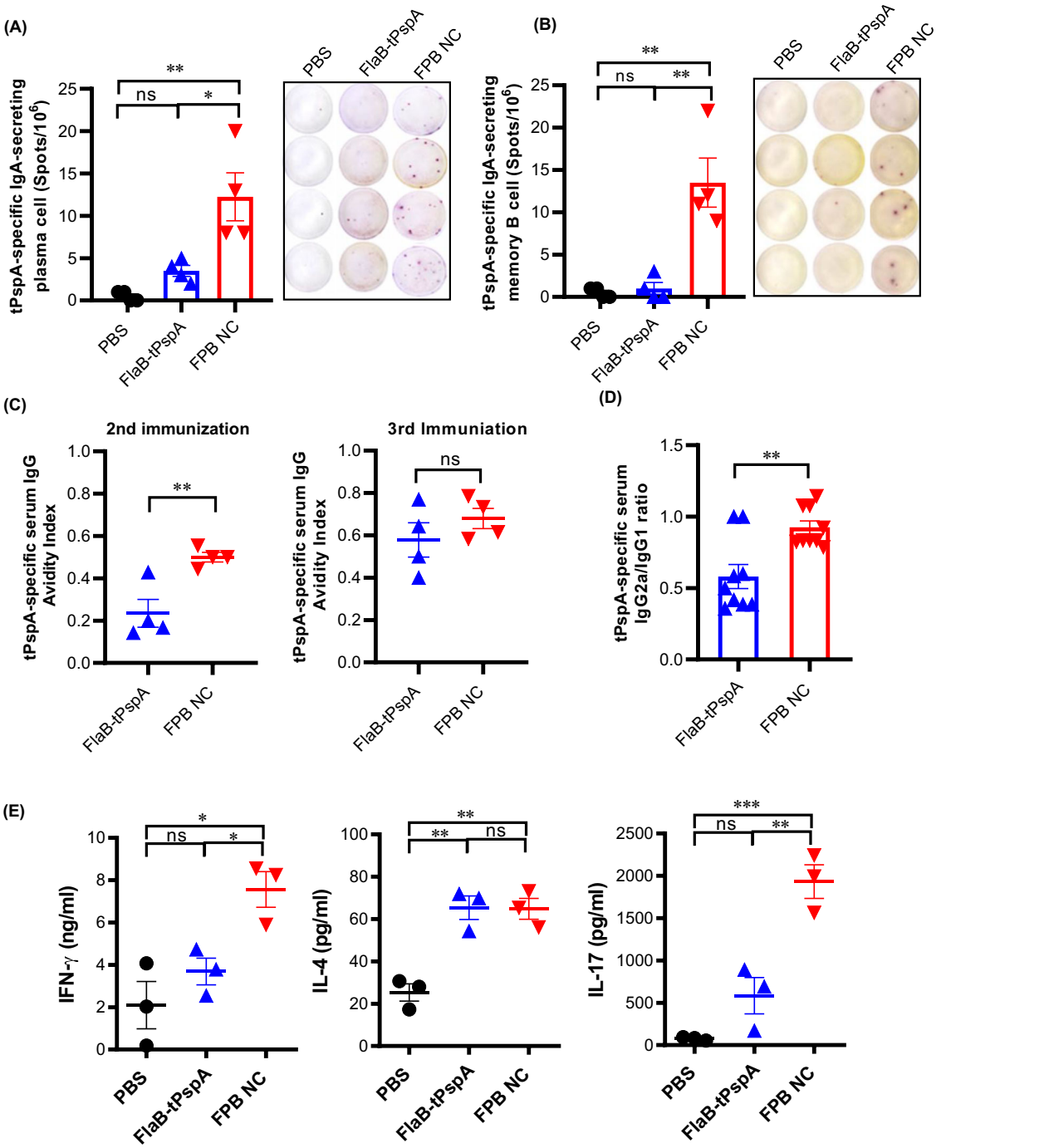

Fig. 4 | High-quality antigen-specific immune responses induced by intranasal (I.N.) immunization of the FPB NC vaccine. Determination of tPspA-specific plasma cells (**A**) and memory B cells (**B**). Two weeks after the final vaccination, tPspA-specific IgA-secreting plasma cells from the bone marrow and memory B cells from the spleen were evaluated via the ELISPOT assay ($n = 4$ biological replicates). Data are presented as mean values ± SEM. Statistical differences were analyzed using one-way ANOVA. Statistical significance: $^{*}P < 0.05$; $^{**}P < 0.01$; $^{****}P < 0.0001$; ns = not significant. Source data are provided as a Source Data file. Detail *P* values are provided in the Source Data file. **C** Determination of the tPspA-specific IgG avidity index. One week after the 2nd and 3rd immunizations, the tPspA-specific serum IgG serum avidity was evaluated using ELISA ($n = 4$ biological replicates). **D** Determination of tPspA-specific serum IgG_{2a}/IgG_1. Two weeks after the final immunization, the tPspA-specific serum IgG_{2a}/IgG_1 ratio was evaluated using an enzyme-linked immunosorbent assay (ELISA) ($n = 9$ biological replicates). Data are presented as mean values ± SEM. Statistical differences between two groups were analyzed using Student's *t*-test. Statistical significance: $^{*}P < 0.05$; $^{**}P < 0.01$; $^{****}P < 0.0001$; ns = not significant. Source data are provided as a Source Data file. Detail *P* values are provided in the Source Data file. **E** Determination of tPspA-specific IFN-γ, IL-4, and IL-17 production. Two weeks after the final immunization, splenocytes were isolated and stimulated with 1 μg/ml of tPspA for three days. Cytokine levels were then measured using ELISA ($n = 3$ biological replicates). Data are presented as mean values ± SEM. Statistical differences were analyzed using one-way ANOVA. Statistical significance: $^{*}P < 0.05$; $^{**}P < 0.01$; $^{****}P < 0.0001$; ns = not significant. Source data are provided as a Source Data file. Detail *P* values are provided in the Source Data file.

https://doi.org/10.1038/s41467-025-58115-8

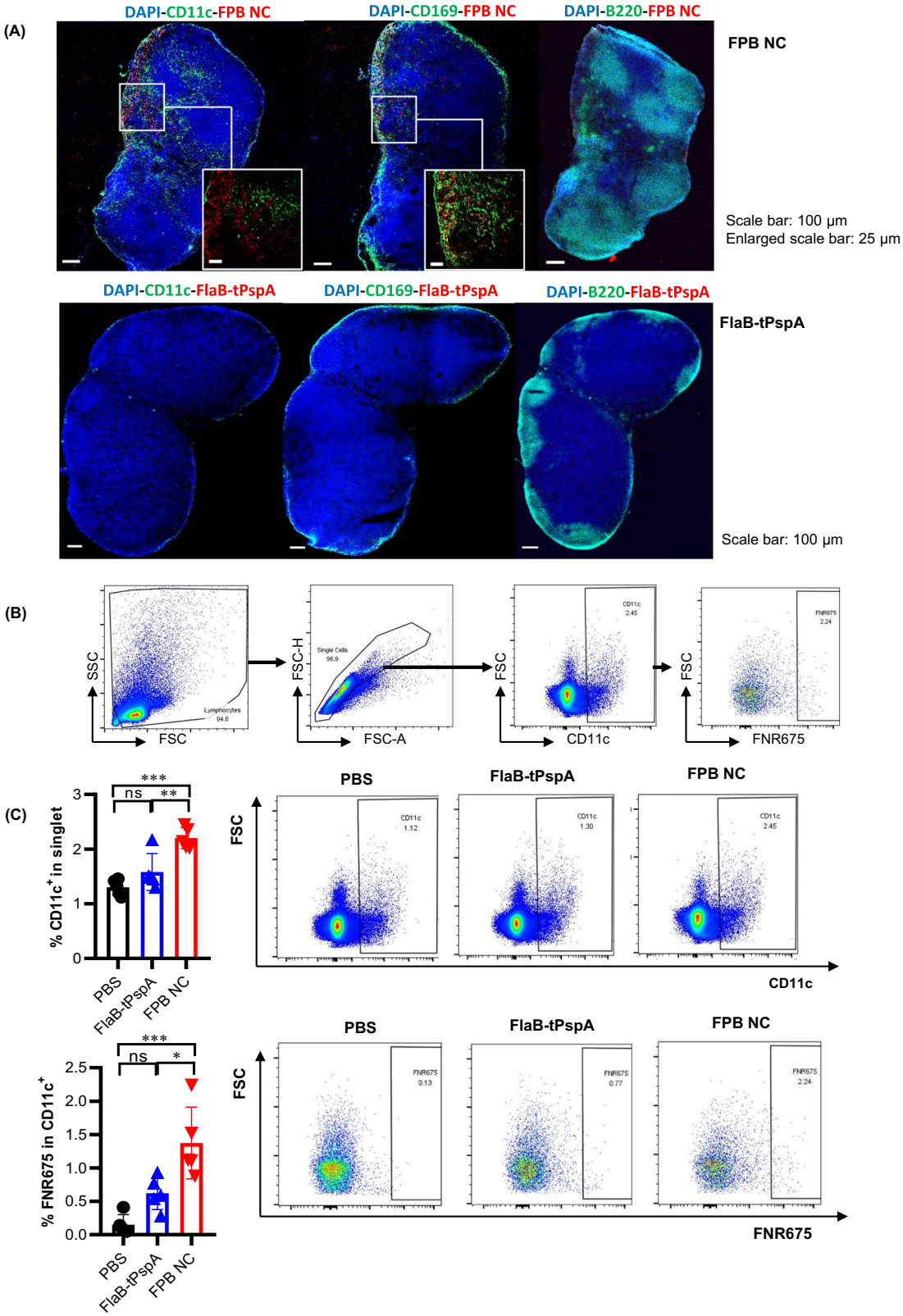

Fig. 5 | Delivery of the FPB NC to the draining lymph nodes. A Observation of the FPB NC delivery to the draining lymph nodes by confocal microscope. Seven-week-old BALB/c mice were subcutaneously (S.C.) immunized in the groin with PBS, 30 μg of FNR675-conjugated FlaB-tPspA, or 30 μg of FNR675-conjugated FPB NC. Three hours after administration, inguinal lymph node (iLN) sections were prepared, and confocal microscopic observation was performed using anti-CD11c, anti-B220, and anti-CD169 antibodies. The most left enlarged image showed the interaction between FPB NC (red) and $CD11c^+$ cells (green). Middle enlarged image showed the interaction between FPB NC (red) and $CD169^+$ (green). Data representative from at least 2 times independent experiments. **B** Gating strategy to determine the percentage of $FNR675^+$ cells within $CD11c^+$ population in mice immunized with FPB NC, FlaB-tPspA and PBS. **C** Determination of the FPB NC delivery in the draining lymph nodes by flow cytometry. Three hours after the administration, iLNs cells were prepared, and flow cytometric analysis was performed ($n = 5$ biological replicates). Data are presented as mean values ± SEM. Statistical differences were analyzed using one-way ANOVA. Statistical significance: $^*P < 0.05$; $^{**}P < 0.01$; $^{****}P < 0.0001$; ns = not significant. Source data are provided as a Source Data file. Detail *P* values are provided in the Source Data file.

the frozen section (Fig. 6A). Tissue sections (7 μm) were cut and placed on charged slides. Tissue sections were stained with markers for FDCs (CD21/35), B cells (B220), activated GC B cells (GL7), and T cells (CD3) (Figs. 6B and S4). GC formation was confirmed by co-localization of B220 and GL7 (Figs. 6B and S4). FPB NC (716.0 ± 61.45 counts) significantly enhanced the GC formation compared to the FlaB-tPspA (418.59 ± 30.73 counts) group Fig. 6C, D). The GC formation by FPB NC administration was abolished in TLR5KO mice (Fig. 6B), suggesting the essential role of the flagellin-TLR5 signaling axis in the GC reactions induced by FPB NC. We also repeated the same experiment in the iLN by only one-time subcutaneous (S.C.) administration. We observed the same results, wherein the FPB NC exhibited significant induction of GC formation, and this effect was abolished in TLR5KO mice (Fig. S5).

Tfh cells help GC B cells through cognate T-B-cell interactions, promoting their proliferation, survival, and differentiation. We also evaluated the Tfh induction by flow cytometry (Fig. 7A). FPB NC (0.219 ± 0.0090%) induced a significantly higher number of Tfh cells compared to FlaB-tPspA (0.138 ± 0.011%) and PBS (0.106 ± 0.018%) groups (Fig. 7B, C), suggesting better support for B cell expansion, activation, and differentiation in the GC.

The FPB NC vaccine significantly enhances protection against lethal challenges

To evaluate the protective efficacy of the FPB NC vaccine, we performed challenge experiments by I.N. infection with lethal doses of *S. pneumoniae* after the final immunization as previously described[24]. Briefly, each BALB/c mouse immunized with FPB NC or FlaB-tPspA was I.N. administered with 1.9 × LD_{50} of live *S. pneumoniae* WU2 or 1.7 × LD_{50} of live *S. pneumoniae* D39. Subsequently, we closely monitored the animals for clinical signs of disease, including weight loss and deterioration in quality of life (Fig. 8A). As shown in Fig. 8B, on the day six following the challenge with the homologous serotype of *S. pneumoniae* WU2, 100% of the FPB NC vaccinees survived (***$P < 0.001$ for PBS vs. FPB NC). Indeed, vaccination with FlaB-tPspA also elicited a significant protective response, as indicated by the 55.6% survival rate observed on day 6 (*$P < 0.05$ compared to the PBS group). The protective efficacy of FPB NC was significantly superior to that of FlaB-tPspA (*$P < 0.05$ for FlaB-tPspA vs. FPB NC). In the challenge experiment with the heterologous serotype *S. pneumoniae* D39, the FPB NC vaccinees showed 100% survival on day 6 (***$P < 0.001$ for PBS vs. FPB NC, Fig. 8C). The FPB NC appeared to be superior to FlaB-tPspA, however this difference was not statistically significant ($P = 0.066$). Although the FlaB-tPspA vaccine resulted in better survival than the PBS control, this difference was also not statistically significant ($P = 0.092$). Furthermore, it is worth noting that in both challenge experiments, quality of life was distinctively better in animals vaccinated with FPB NC. The FPB NC-vaccinated group did not manifest conspicuously severe symptoms, such as rapid heart rate, lethargy, or ruffled fur. In contrast, the FlaB-tPspA group displayed mild symptoms, while the PBS group experienced pronounced morbidity (Supplementary Movie 2, 3). These results demonstrate that compared with the FlaB-tPspA fusion protein vaccine, the FPB NC vaccine significantly enhances protection against lethal challenges with both homologous and heterologous *S. pneumoniae* strains. The FPB NC vaccine induces more excellent avidity antibody responses and a more comprehensive range (cross-protective) of protective immune responses.

To investigate how significantly improved protection was conferred by the FPB NC vaccination compared with FlaB-tPspA, we assessed the bacterial load in lung tissue, bronchoalveolar lavage fluid (BAL-F), and blood. Briefly, Balb/c mice were intranasally immunized three times with either the FlaB-tPspA fusion protein or FPB NC. Two weeks after the final immunization, the mice were intranasally challenged with live *S. pneumoniae* WU2 (0.6×10^8 CFU/mouse; 0.6 × LD_{50}). Seventy-two hours post-challenge, pneumococcal colony-forming units (CFU) were determined in the lung tissue, BAL-F, and blood. Additionally, the presence of pneumococci in these compartments was also quantified using qPCR with primers targeting the 16S rRNA gene. In contrast to the non-vaccinated PBS control group (5.707 ± 0.244; $\log_{10}$ CFU/g) or the FlaB-tPspA (4.290 ± 0.696 $\log_{10}$ CFU/g) vaccinated group (PBS vs. FlaB-tPspA: ns $P > 0.05$), no colony-forming bacteria were detected in the lung tissue of FPB NC-vaccinated mice (PBS vs. FPB NC: ****$P < 0.0001$; FlaB-tPspA vs. FPB NC: **$P < 0.01$) (Fig. 8D). These results indicate that the FPB NC vaccine induced more robust protective immune responses than the FlaB-tPspA vaccine, which effectively suppressed *S. pneumoniae* growth in the lung. The qPCR data recapitulated colony-forming bacterial count results: the FPB NC group (4.130 ± 0.294; $\log_{10}$ counts/g) also showed a significant reduction in bacterial load compared to the FlaB-tPspA group (6.537 ± 0.511; $\log_{10}$ counts/g) (FlaB-tPspA vs FPB NC: **$P < 0.01$) (Fig. S8A). Bacterial counts in BAL-F samples are similar to those of lung tissue (Figs. 8D and S8A). Upon challenging the PBS control mice with live *S. pneumoniae* WU2 72 h post-intranasal infection, a bacterial load of 5.93 ± 0.42 ($\log_{10}$ CFU/ml) was detected in the blood. This result confirmed the invasiveness of the WU2 strain to the bloodstream. The CFU and qPCR experiments could not detect a trace of bacteria in the blood of the FlaB-tPspA or FPB NC vaccinated group (below detection limits) (Figs. 8D and S6A), indicating that both vaccinations effectively inhibited bacterial invasion into the bloodstream. Upon histological examination of lung tissue following BAL-F preparation, the FPB NC-vaccinated group showed less lung injury than the other groups, notably reduced parenchymal inflammation and bronchitis features (original magnification 200X) (Fig. S6B). Taken together, the FPB NC vaccine induced both quantitively and qualitatively enhanced protective immune responses compared with the FlaB-tPspA vaccine, which significantly reduced bacterial load in the lower respiratory tract and prevented subsequent invasion into the bloodstream.

Discussion

In this study, we introduce the development of a protein-based nanocage mucosal vaccine platform that can simultaneously display antigens and adjuvants in multivalency. To this end, we have utilized the 24-mer ferritin nanocages providing multivalency and a SpyTag/SpyCatcher system, allowing the fusion of proteins to ferritin subunits. This system could also modulate the ratios of different components (antigens/epitopes and adjuvants) and the valency of antigenic determinants. In the present study, we have used a truncated fragment of *S. pneumoniae* PspA as an antigen and the mucosal adjuvant FlaB, which was previously well-tested in the laboratory[24,57], and we established a nanocage vaccine platform named FPB NC and compared it with the FlaB-tPspA fusion formulation. The results were remarkable: the FPB NC vaccine induced significantly enhanced sIgA responses in the mucosal compartments and a well-balanced systemic Th1/Th2 immune modulation, leading to a significantly improved protection against *S. pneumoniae* infection compared with FlaB-tPspA. This finding underscores the potential of the FPB NC vaccine in combating S. pneumoniae infection.

Ferritin nanocages have emerged as a promising platform for vaccine development, primarily owing to their biocompatibility, stability, and capacity to encapsulate and display antigenic peptides or proteins to the immune system[6,9]. A study has been published presenting a ferritin nanoparticle-based, SpyTag/SpyCatcher-enabled click vaccine platform, particularly aimed at personalized tumor immunotherapy[29]. Ferritin nanocage platforms have been applied for developing more efficacious vaccines against a broad spectrum of infectious agents, including HIV, influenza, RSV, malaria, *Pseudomonas aeruginosa*, hepatitis B, and SARS-CoV-2, in an attempt to present multivalent antigens with higher stability[7,8,34,57–60]. Covalent fusion of antigen peptides/proteins to ferritin should ensure the stable display of antigens on ferritin nanoparticles for the recognition by antigen-

https://doi.org/10.1038/s41467-025-58115-8

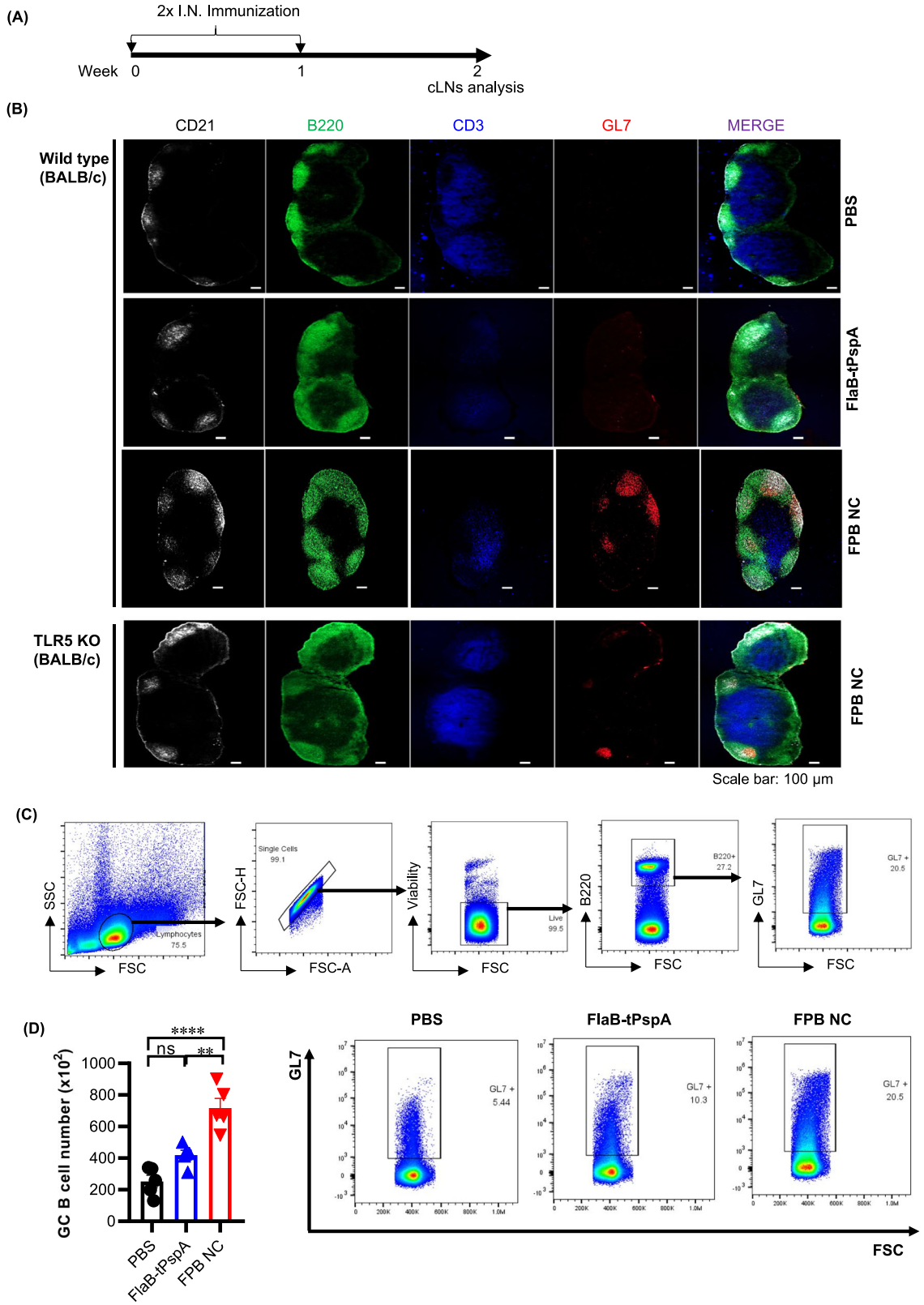

Fig. 6 | Germinal center formation by intranasal (I.N.) immunization of the FPB NC vaccine. A Experimental schedule for immunization. BALB/c mice were intranasally (I.N.) immunized with PBS, 50 μg of FlaB-tPspA, or 50 μg of FPB NC two times at one-week intervals for a total volume of 20 μl per mouse. **B** Immunofluorescence staining of cervical lymph nodes (cLNs). One week after the last administration, cLN sections were prepared, and confocal microscopic observation was performed using anti-CD21, anti-B220, anti-CD3, and anti-GL7 antibodies. Data representative from at least 2 times independent experiments. **C** Gating strategy to determine the percentage of $GL7^+$ cells within $B220^+$ population in mice immunized with FPB NC, FlaB-tPspA and PBS. **D** Detection of germinal center B cell by flow cytometry. One week after the last administration, cLNs cells were prepared, and absolute numbers of $B220^+$ $GL7^+$ in cLNs were analyzed by flow cytometry ($n = 5$ biological repllicates). Data are presented as mean values ± SEM. Statistical differences were analyzed using one-way ANOVA. Statistical significance: $^*P < 0.05$; $^{**}P < 0.01$; $^{****}P < 0.0001$; ns = not significant. Source data are provided as a Source Data file. Detail *P* values are provided in the Source Data file.

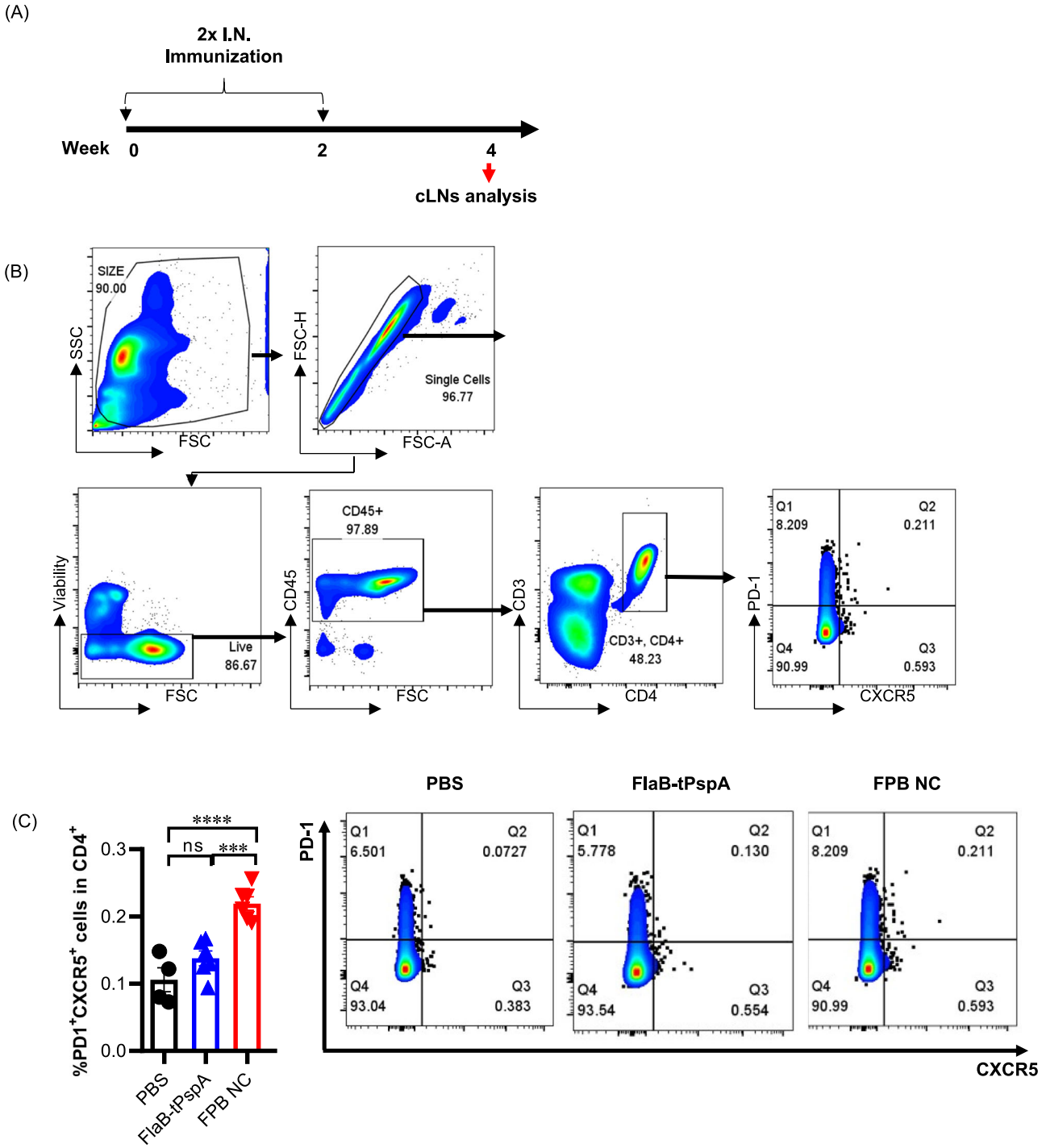

Fig. 7 | The follicular helper T cell (Tfh) expansion in the draining lymph nodes by intranasal (I.N.) immunization of the FPB NC vaccine. A Experimental schedule for immunization. BALB/c mice were intranasally (I.N.) immunized with PBS, 6.5 μg of FlaB-tPspA, or 14.5 μg of FPB NC two times at two-week intervals for a total volume of 20 μl per mouse. **B** Gating strategy to determine the percentage of PD−1$^+$ CXCR5$^+$ cells within CD3$^+$ CD4$^+$ population in mice immunized with FPB NC, FlaB-tPspA and PBS. **C** Detection of Tfhs by flow cytometry. Two weeks after the last administration, cLNs cells were prepared, and flow cytometric analysis was performed ($n = 6$ biological replicates). Data are presented as mean values ± SEM. Statistical differences were analyzed using one-way ANOVA. Statistical significance: $^*P < 0.05$; $^{**}P < 0.01$; $^{****}P < 0.0001$; ns = not significant. Source data are provided as a Source Data file. Detail *P* values are provided in the Source Data file.

presenting cells and B cells in a multivalent manner. This may be a limitation of displaying two or more heterologous proteins on ferritin nanocages. However, the SpyTag/SpyCatcher system, a covalent protein coupling technology, provides an efficient and specific solution for displaying heterologous proteins on ferritin nanocages in a controlled fashion[26–28]. In most ferritin nanocage vaccine platform studies, antigen peptides were shown using the SpyTag/SpyCatcher system since direct fusion of antigens to the N- or C-terminus often results in significantly lower expression[9]. This versatility of the SpyTag/SpyCatcher system reassures us of the adaptability and potential of the ferritin nanocage platform in vaccine development.

In our study, SpyTag was fused to the N-terminus of ferritin, and SpyCatcher was fused to the tPspA antigen or FlaB adjuvant to generate a built-in adjuvanted nanoparticle vaccine named FPB NC. Using

https://doi.org/10.1038/s41467-025-58115-8

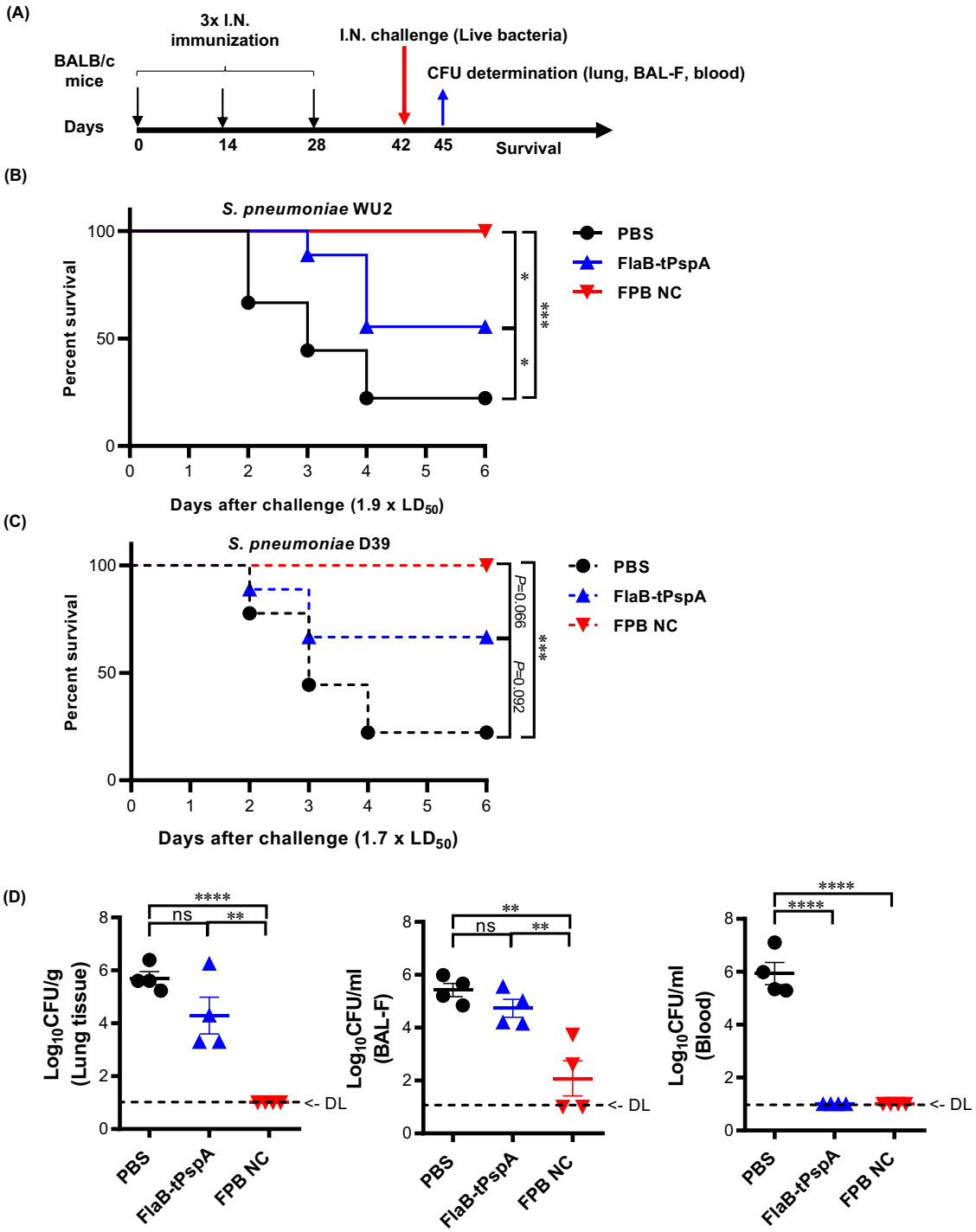

Fig. 8 | Protection against live *Streptococcus pneumoniae* infection by intranasal vaccination. A Experimental schedule of lethal challenge with live *S. pneumoniae*. Determination of the protective immune response against lethal challenge with *S. pneumonia* WU2 (**B**) or D39 (**C**) strain. Groups of mice were intranasally (I.N.) vaccinated with PBS, 6.5 µg of FlaB-tPspA, or 14.5 µg of FPB NC three times at two-week intervals. Two weeks after the last immunization, the immunized mice were I.N. challenged with a 1.9 x LD_{50} of live *S. pneumoniae* WU2 ($n = 9$ biological replicates) or a 1.7 x LD_{50} of live *S. pneumoniae* D39 ($n = 10$ biological replicates) separately. After the challenge, the survival rate was monitored. Statistical differences were analyzed by the log-rank (Mantel-Cox) test. **D** Determination of pneumococcal colony-forming units (CFU) in lung tissue, bronchoalveolar lavage fluid (BAL-F), and blood samples. Two weeks after the final immunization, mice were intranasally challenged with live *S. pneumoniae* WU2 (0.6×10^8 CFU/mouse; $0.6 \times LD_{50}$). Seventy-two hours post-challenge, pneumococcal CFU was quantified in lung tissue, BAL-F, and blood samples ($n = 4$ biological replicates). Data are presented as mean values ± SEM. Statistical differences were analyzed using one-way ANOVA. Statistical significance: $^*P < 0.05$; $^{**}P < 0.01$; $^{****}P < 0.0001$; ns = not significant. Source data are provided as a Source Data file. Detail *P* values are provided in the Source Data file.

this nanocage vaccine, we aimed to stimulate the same antigen-presenting cell (APC) with both adjuvant and antigen, which is expected to result in more efficient antigen-specific immune responses. Notably, the TLR5-dependent NFκB activation induced by FPB NC was more than that caused by recombinant FlaB. This suggests that FlaB maintains its structure intact when displayed on the ferritin nanocages. The TLR5 binding sites are more readily accessible than recombinant FlaB, which tends to polymerize in its natural structure. The virtually simulated structure suggested that the TLR5-binding domains of FlaB monomers extend from the ferritin nanocage core (Fig. 1A and Supplementary Movie 1). This should enable FPB NC to stimulate TLR5 expressing DCs in multivalency, resulting in more robust activation. The size of FPB NC, measured at 24.8 ± 6.3 nm (Fig. 2D), falls within the optimal range for the uptake by APCs. Considering that nanoparticles ranging from 10 to 200 nm in size efficiently translocate to draining LNs and remain there for an extended duration[52], FPB NC could facilitate the maturation of FDCs and the subsequent formation of a GC within the LN[50]. It was evident that FPB NC reached dLNs with a greater propensity, where it appeared to be taken up by $CD11c^+$ APCs (Fig. 5). Notably, a greater frequency of germinal center B cells was observed in the B-cell areas of the draining lymph nodes in the group administered with FPB NC compared to the group receiving the FlaB-tPspA fusion protein (Fig. 6). Upon reaching B cells, the antigens and adjuvants on FPB nanocages are likely recognized in a multivalent manner, which intensifies B-cell receptor crosslinking and downstream signaling, alongside TLR5-mediated innate immune activation. These processes likely enhance antibody responses in both quantity and quality, as indicated by higher antibody titers and avidity, respectively (Figs. 3 and 4).

Th1 cells are primarily involved in the cellular immune response and are responsible for activating macrophages, which are critical immune cells that engulf and destroy pathogens. Some evidence suggests that *S. pneumoniae* can be internalized and replicated within specific host cells, such as $MRC1^+$ alveolar macrophages, DCs, or $CD169^+$splenic macrophages[61,62]. This intracellular persistence has been suggested to play a role in the pathogenesis of pneumococcal infections in both pneumonia and meningitis. Therefore, the Th1 response should be critical in eradicating intracellular persistence. A previous study[24] showed that the FlaB-tPspA fusion vaccine had good protective efficacy against *S. pneumoniae in* a mouse model. However, while this direct fusion protein vaccine potentiated the anti-tPspA antibody responses in both mucosal and systemic immune compartments, it weakly induced Th1 responses. In this mouse model, the FPB NC induced more balanced immune responses than did FlaB-tPspA (Fig. 4D, E). Considering the results obtained from our mouse model system, it may be worth exploring the potential clinical application of the multivalent ferritin nanocage vaccine, which incorporates a built-in flagellin adjuvant, in developing vaccines targeting pneumococcal PspA. While further studies are necessary, this platform could offer advantages in achieving more balanced immune responses for such vaccines, even with mucosal vaccination.

IL-17 plays an important role in protecting barrier surfaces against extracellular bacterial and fungal pathogens[63]. The most important physiological function of IL-17 is the induction of chemokines, including CXCL1, CXCL2, and CXCL8 (IL-8), attracting myeloid cells such as neutrophils to the infection sites. Infiltrating myeloid cells, together with phagocytosis of infecting pathogens, secret antimicrobial peptides such as β-defensins, S100A8, and lipocalin 2, which exert additional protection of the host during acute microbial invasion[63]. Th17 response is reported to play a crucial role in eradicating pneumococcal colonization in the upper airway[64]. Th17 cells are preferentially induced by protein antigens and cross-protective against various capsular serotypes[65,66]. For the protection against pneumococcal pneumonia and systemic spreading, it is known that both antibodies and Th17 cells in both mouse models and humans[65]. In this regard, new pneumococcal vaccine design efforts should aim to induce more robust Th17 responses[67]. In the present study, the FPB NC vaccine potently induced IL-17 responses and strong antigen-specific antibody responses (sIgA in respiratory secretion and IgG in serum). Induction of both might explain the markedly potentiated protective potential of FPB NC against pneumonia and invasion into the bloodstream. The difference in IL-17 response between FPB NC and FlaB-tPspA groups should explain why FPB NC vaccination showed a marked reduction of CFU in lung tissue and BAL-F (Figs. 4E and 8D). Unfortunately, we could not assess the effects on colonization because our experimental model did not allow counting live pneumococcal cells for extended periods with lower dosages of intranasal infection[67].

The presence of antigen-specific memory B cells is a distinct measure of vaccine effectiveness and is closely correlated with antibody recall responses. In our study, compared with FlaB-tPspA, FPB NC strongly induced IgA-specific memory B cells and long-lived plasma cells compared with FlaB-tPspA. This suggests that our nanocage vaccine can establish longer-lasting antibody responses with higher avidity in both the portal of entry and systemic compartment. After the I.N. challenge with a lethal dose of live pathogenic *S. pneumoniae*, the FPB NC group exhibited significantly longer survival and better quality of life than the FlaB-tPspA group (Fig. 8, Supplementary Movie 2, 3). This result suggests that our vaccine candidate shows promise in preclinical models; however, further studies are required to compare its efficacy with currently licensed pneumococcal vaccines directly.

The ferritin nanoparticle influenza vaccine was subjected to a phase 1 clinical trial (ClinicalTrials.gov NCT03186781 and NCT 03814720) as a single or a prime-boost regimen[7]. Both vaccine regimens were safe and well tolerated, broadly neutralizing antibody responses. These results corroborate the clinical applicability of ferritin-based nanoparticle vaccines[68]. However, most of those vaccines were administered by injections formulated with adjuvants, which may not fully replicate what we have seen through the mucosal immunization of FPB NC. A self-assembling influenza nanoparticle adjuvanted with AddaVax, administered intramuscularly to C57BL/6 mice, appeared to drive extended germinal center activity and memory B cell maturation, similar to our FPB NC vaccine[69]. However, enhanced immunogenicity of the same vaccine was not noted in pigtail macaques, where antibody titers and LN reactions were similar to soluble vaccines[69]. Before being translated into clinical studies, our built-in flagellin adjuvanted mucosal vaccine platform should also be verified with other animal models and antigen combinations. The ferritin nanoparticle influenza clinical trial employed a non-adjuvanted formulation[7], while preclinical studies were carried out in combination with the Ribi emulsion adjuvant with dramatically enhanced potency and cross-protection[8]. Our platform comprises a built-in adjuvant whose incorporation ratio could be titrated depending on the number and immunogenicity of accompanying antigens. This would provide more versatility in manufacturing clinically applicable production.

Methods

Ethics approval and consent to participate

The Chonnam National University Institutional Animal Care and Use Committee, approved all animal experimental procedures under the protocol CNU IACUC-H-2022-44. For ethical reasons, mice that exhibited a loss of body weight exceeding 20% and ceased to consume food and water were humanely euthanized, serving as an endpoint to minimize any potential distress. Mice were euthanized by carbon dioxide inhalation using a euthanasia station with a dedicated chamber, compressed gas cylinder, and regulated flow rate combined with subsequent cervical dislocation of apparent dead animals. The animal research facility and experimental procedures strictly adhered to the

guidelines of the Animal Welfare Act enacted by the Korean Ministry of Agriculture, Food, and Rural Affairs.

Mice

BALB/c female mice (7 weeks, stock number: AnNCrlOri-7WKS), weighing 20–25 g, were obtained from Orient Bio Inc. (Seongnam, Gyeonggi-do, Korea) and were acclimatized in a temperature (20 °C) and humidity (50%) controlled environment with a 12–12 h light-dark cycle. Mice were housed for one week with ad libitum access to food and water before their distribution in three groups. Experimental group sizes were approved by the regulatory authorities for animal welfare after being defined to balance statistical power, feasibility, and ethical aspects. All experimental murine were housed in specific-pathogen-free (SPF) barrier facilities, except TLR5 KO Balb/c mice were bred separately and adapted in SPF barrier facility one week before doing experiments.

Bacterial strains, plasmids, and culture conditions

The bacterial strains and plasmids used in this study are listed in Table S1. *S. pneumoniae* strains were routinely cultured in Todd-Hewitt broth (Cat: 249240, Becton Dickinson and Co., Le Pont de Claix, France) supplemented with 5% yeast extract (Cat: 212750, BD) or on 5% sheep blood agar plates (Cat:MB-S1876, MB Cell) at 37 °C under 5% CO_2. Plasmids were maintained using *Escherichia coli* cells grown on Luria Bertani (LB) agar plates (244620, BD) supplemented with an antibiotic: ampicillin (100 μg/ml) (Cat: AC1043-025-00, Biosesang) or kanamycin (100 μg/ml) (Cat: K1377-25G, Sigma Aldrich).

Construction and purification of recombinant proteins for nanocage formulation

The constructs were cloned using standard PCR methods and ligation. Inserts were verified by Sanger sequencing. In all cases, the version of SpyCatcher used was ΔN1-SpyCatcher[31], and Ftn from *Pyrococcus furious* was chosen because of its thermostability[70]. The ΔN1-Spycatcher (SC)::$(G_4S)_3$ and *spytag*(ST)::$(G_4S)_3$::*ftn* genes were subjected to codon optimization for the expression in *E. coli* and were synthesized by Macrogen (Macrogen, Inc., Seoul, Korea). The tPspA construct encompassing amino acid residues 3 to 236, corresponding to the alpha-helical region of the mature Rx1 PspA protein, was used as an antigen[24,71,72]. The corresponding *pspA* DNA fragment was amplified and ligated to the C-terminal end of SC::$(G_4S)_3$ within the pET30a(+) vector (Fig. 1A). This process was carried out by using the primer pair tpspA-F/tpspA-R (Table S2). Then, the SC::$(G_4S)_3$::*tpspA* DNA fragment was amplified and inserted into the pTYB12 plasmid through subcloning using the primer pair SC-F/tpspA-R (Table S2). The DNA fragment corresponding to *V. vulnificus flaB* was amplified and subsequently fused to the C-terminal end of ΔN1-SC with the inclusion of a flexible linker $(G_4S)_3$. The *flaB* DNA fragment was subcloned and inserted into the pET30a(+) vector utilizing a pair of primers designated as flaB-F/flaB-R (Table S2). Furthermore, the DNA fragment of ST::$(G_4S)_3$::*ftn* was amplified and integrated into the pET30a(+) plasmid using the primer pair ST-F/ftn-R (Table S2). Sanger sequencing (Macrogen, Inc., Seoul, Korea) confirmed the DNA sequences of the resulting expression vectors. Plasmids were maintained in *E. coli* grown on Luria-Bertani (LB) agar plates supplemented with ampicillin (100 μg/ml) or kanamycin (100 μg/ml). The constructs were expressed in *E. coli* BL21.Competent *E. coli* BL21 cells were individually transformed with the following plasmids: pET-30a(+)::SC::*flaB*, pET-30a(+)::ST::*ftn*, or pTYB12::SC::*tpspA*. Protein expression was initiated when the optical density at 600 nm (OD_{600}) reached 0.6; at this point, one mM isopropyl-D-thiogalactopyranoside (IPTG) (Cat: 367-93-1, Duchefa Biochemie) was added. Incubation was subsequently conducted under controlled conditions. For SC-tPspA and SC-FlaB expression, cells were incubated at 18 °C for 16 h, while ST-Ftn expressing cells were incubated at 37 °C for 4 h. Following incubation, the cells were harvested by centrifugation at 11,000 × g for 10 min and stored at −80 °C until further use. SC-FlaB was purified using a Ni-affinity column (Cat: 30230, Qiagen). The resulting pellet was reconstituted in a lysis buffer composed of 50 mM NaH_2PO_4 (pH=8.0), 300 mM NaCl, ten mM imidazole (Cat: A10221.36, Thermoscientific), 0.1% Triton X-100 (Cat: 93422, Sigma Aldrich), 0.1% Tween 20 (Cat: P6585, Sigma Aldrich), and 20 mM phenylmethylsulfonyl fluoride (PMSF) (Cat: 329-98-6, Merck). Sonication was performed using a sonicator (Vibra Cell VCX500; Sonics & Materials, Inc., Newtown, CT) in an ice bath. Subsequently, the suspension was centrifuged at 37,000 × g for 30 min. The resulting cell-free supernatant was then applied to a column filled with Ni-NTA agarose beads (Qiagen, Hilden, Germany). The purity of the recombinant proteins was confirmed by sodium dodecyl sulfate-polyacrylamide gel electrophoresis (SDS–PAGE). For the ST-Ftn purification, the bacterial pellet was reconstituted in a lysis buffer of 20 mM Tris-HCl, 50 mM NaCl, and 20 mM PMSF (pH 7.5). Sonication was performed on an ice bed. Following centrifugation, the protein concentration of the supernatant was quantified and subsequently adjusted to the concentration of 1 mg/ml. After dilution, the supernatant was heated at 70 °C for 15 min to dissociate the aggregates. After this step, the aggregate-free solution was isolated through centrifugation. The soluble protein in the heated supernatant was concentrated and introduced into a Superose 6 column (Cat: 29-3239-52, GE Healthcare) in the same lysis buffer. For SC-tPspA purification, the pellet was suspended in a lysis buffer (pH 7.5) of 20 mM Tris-HCl, 500 mM NaCl, and one mM EDTA (Cat:84125S0350, Junsei). Subsequently, the suspension was subjected to sonication and centrifugation. According to the manufacturer's instructions, the supernatant was applied to a column filled with chitin agarose beads (Cat: S6651L, New England Biolabs).

Optimization and purification of nanocage vaccine

For the assembly of the ferritin-tPspA-FlaB nanocage (FPB NC), the components ST-Ftn, SC-tPspA, and SC-FlaB were mixed in different ratios. The optimal ratio for animal studies was determined based on stability and TLR5 stimulation activity. The mixture was incubated at 4 °C overnight. On a subsequent day, this mixture was dialyzed in buffer A (comprising 50 mM Tris-HCl at pH 8.0 and 20 mM NaCl) for 2 h at 4 °C. The solution was introduced into a Q anion exchange column (Cat: 17115401, Cytiva) after the dialysis. The protein nanocage fractions were isolated, and the buffer was exchanged with phosphate-buffered saline (PBS) using centrifugal filter tubes (Cat: UFC9010, Ultra15 Centrifugal Filter, 10k, Merck). Lipopolysaccharide (LPS) contamination was removed by treatment with Triton X-114 (Sigma Aldrich, St. Louis, MO). To eliminate residual traces of Triton X-114, the protein samples were treated with Bio-Beads™ SM-2 (Cat: 1523920, Bio-Rad Laboratories, Inc., Hercules, CA) following the manufacturer's instructions. The remaining LPS was quantified using a gel-clotting EndoSafe LAL kit (Cat: G5006-5, Pyrotell). The LPS levels within the protein preparations were maintained below the Food and Drug Administration (FDA) guidelines (less than 0.15 EU/30 g per mouse). For the assembly of the Ferritin-FlaB nanocage (FB NC) and ferritin-tPspA nanocage (FP NC), the ST-Ftn components were mixed with SC-FlaB or SC-tPspA in a 1:1.5 ratio. The mixtures were incubated at 4 °C overnight. Subsequent purification and endotoxin removal steps were performed identically to those used in preparing FPB NC.

3D simulation of the FPB nanocage

For further structural analyses at the molecular level, we constructed a three-dimensional model of the FPB nanocage. Monomeric structures of tPspA-Ferritin and FlaB-Ferritin were built using AlphaFold2 and assembled onto a ferritin multimer structure (PDB ID: 2JD6). GROMACS was employed to remove potential steric clashes. The OPLS-AA/L force field was used with ionized SPC/E water (580 NA +) placed in a cube box with an extension of 10 Å. Pre-equilibration was carried out to

eliminate any physicochemical contacts that were not feasible and to establish a reliable starting point for the simulations. The ST-Ftn:SC-tPspA:SC-FlaB=24:10:10 system underwent the steepest descent energy minimization of 50,000 steps. During this process, restraints were applied to the backbone atoms with a force constant of 1000 kcal/mol^{-1}Å^{-2}. Following the energy minimization, 100-picosecond NVT and NPT equilibrations were conducted. The molecular dynamic (MD) running was performed for one nanosecond, allowing for the collection of relevant data and observations.

SDS-PAGE, native PAGE, and western blotting

The purity of the recombinant proteins was confirmed by SDS–PAGE and native-PAGE. The recombinant proteins were separated by SDS–PAGE for western blotting and transferred onto nitrocellulose membranes (Cat: 10600004, Cytiva). Anti-sera or commercial antibodies were diluted in PBS with 0.05% Tween-20 and were incubated with the respective membranes for 2 h at room temperature (RT) to probe corresponding proteins. The horseradish peroxidase (HRP)-conjugated secondary antibody (Cat: P0260, Agilent) Following the manufacturer's instructions, Dako (Cat: WBKLS0500, Millipore) was used to visualize proteins. All uncropped and unprocessed images were supplied in the Supplementary Information.

Characterization of the nanocage vaccine

The size distribution of nanocages was determined by dynamic light scattering (DLS) analysis using a Zetasizer Nano Z instrument (Malvern Instruments, Malvern, UK). The nanocages were diluted in PBS (pH 7.4). Field emission transmission electron microscopy (FE-TEM) was performed to observe the morphology using a JEM-2100F microscope (JEOL Ltd, Japan). The nanocage concentration for FE-TEM analysis was 0.2 mg/ml, and negative staining of the nanoparticles was carried out using phosphotungstic acid.

Determination of TLR5-dependent NFκB activation

To evaluate the TLR5 stimulation activity of the nanocage vaccine, a luciferase reporter assay for TLR5 signaling was conducted as previously described[25]. Briefly, HEK293T cells were seeded at a density of 2 × 10^5 cells/well in 24-well plates and incubated overnight. The cells were then transfected with p3xFlag-hTLR5 (100 ng/well), the reporter plasmid pNFκβ luc (100 ng/well), and pCMV-β-Gal (50 ng/well) (BD Biosciences Lontech, Palo Alto, CA, USA) using five μl/well of Effectene transfection reagent (Cat: 301427, Qiagen). After 24 h of transfection, the cells were treated with purified recombinant proteins and nanocages overnight, and the molar ratio was adjusted to ensure equivalent amounts of FlaB per well. Transfected cells treated with PBS served as a negative control. After overnight treatment, the cells were lysed using a lysis buffer (Promega, E153A), and the luciferase activity was quantified using a luminometer (MicroLumat-Plus LB 96 V, Berthold, Wilbad, Germany). The TLR5-stimulated luciferase signals for each sample were assessed as the fold-change in activity relative to that of the negative control.

Intranasal immunization

Seven-week-old female BALB/c mice (stock number: 7WKS) were used. Mice were intranasally immunized three times at 2-week intervals with either PBS, 6.5 μg of FlaB-tPspA, or 14.5 μg of the Ftn-tPspA-FlaB nanocage (FPB NC) in a volume of 20 μl. Immunizations were conducted under anesthesia[25]. Two weeks after the final vaccination, serum, bronchoalveolar lavage fluid (BAL-F), nasal wash, and saliva samples were collected and preserved at −80 °C until use.

Determination of *Streptococcus pneumoniae* LD_{50}

S. pneumoniae strains were preserved at −80 °C in 15% glycerol (Cat: 27210S0350, Junsei). For each experiment, bacterial strains were streaked onto 5% sheep blood agar plates and incubated for 24 h at 37 °C under 5% CO_2. For overnight liquid culture, 3–10 colonies were inoculated into 5 ml of THY medium supplemented with 5% FBS (Biochrom KG, Berlin, Germany) using a 15 ml culture tube (Sarstedt AG, St. Gallen, Switzerland) and incubated at 37 °C under 5% CO_2 overnight. Subsequently, a subculture was performed by transferring 100 μl of the overnight culture into 5 ml of fresh THY broth supplemented with 5% FBS, and the culture was grown until the mid-log phase (OD_{600} 0.6–0.8).

Determination of the LD_{50} of *S. pneumoniae* D39 and WU2 strains was carried out using twelve-week-old specific-pathogen-free (SPF) female BALB/c mice[24]. The cell pellet from the exponentially grown culture described above was resuspended and diluted with THY medium containing 5% FBS. Mice were intranasally infected using 20 μl of *S. pneumoniae* cell suspensions serially diluted in 10-fold increments. Each group consisted of five mice, and their survival was monitored for six days. The LD_{50} was calculated using the Reed and Muench method[24].

Challenge of vaccinated mice with live *Streptococcus pneumoniae*

Two weeks after the final immunization, the mice were subjected to challenge infection with live pneumococci. Mice were intranasally infected with 20 μl of lethal doses equivalent to 1.9 times the LD_{50} of *S. pneumoniae* WU2 and 1.7 times the LD_{50} of *S. pneumoniae* D39[24]. The optimal lethal challenge doses, which should differentially manifest efficacy of protection, were estimated by many rounds of pilot studies. The mice were observed for six days and monitored for mortality and body weight changes.

Determination of colony-forming units of *S. pneumoniae* in various compartments

To evaluate the colony-forming units (CFUs) of live *Streptococcus pneumoniae*, we performed bacterial viable cell counting on lung tissue, bronchoalveolar lavage fluid (BAL-F), and blood samples. BALB/c mice were intranasally immunized three times with either the FlaB-tPspA fusion protein or the FPB nanocage (FPB NC). Two weeks after the final immunization, the mice were intranasally challenged with live *S. pneumoniae* WU2 (0.6×10^8 CFU/mouse; 0.6 × LD_{50}). Seventy-two hours post-challenge, samples were serially diluted and plated on sheep blood agar plates. CFUs were counted after overnight incubation.

Determination of antigen-specific antibodies by ELISA

To determine antigen-specific antibody (Ab) responses, serum, BAL-F, nasal washes, and saliva were collected from immunized mice. ELISA plates (Cat: 3690, Corning Laboratories, Sigma Aldrich, St. Louis, MO) were coated with tPspA antigens (2 μg/ml) in PBS and incubated at 4 °C for 24 h. After washing with sterile distilled water (DW) to remove the unbound antigen, the plates were treated with blocking buffer [0.5% BSA (Cat: A2153, Sigma Aldrich, St. Louis, MO) and one mM EDTA (Bioneer, Korea) in PBST] at room temperature for 1 h. Serially diluted samples in blocking buffer were added to the plates and incubated for 2 h at room temperature, followed by five washes. HRP-conjugated anti-mouse IgG or IgA antibodies were used as secondary antibodies (Table S3). The signal was developed using 40 μl of 3,3′,5,5′-tetramethylbenzidine (TMB) substrate (BD, Franklin Lakes, NJ). The reaction was stopped by adding 40 μl of 1 N H_2SO_4. Optical density measured at 450 nm (OD_{450}) was measured using a microplate reader (Molecular Devices Corp., Menlo Park, CA). Titers are presented as the reciprocal log2 value of the dilution, resulting in OD_{450} values that were 2-fold more significant than the blank well with no serum.

Detection of antibody-secreting cells by ELISPOT

To assess tPspA-specific B-cell responses following three immunizations with the nanocage vaccine, we quantified IgA-secreting plasma

cells in the bone marrow and memory B cells in the spleen as previously described[73]. Briefly, multiscreen 96-well plates (BD Biosciences) were coated with recombinant tPspA (50 μg/ml) overnight at 4 °C. After blocking with RPMI 1640 (Cat: 11875-093, Gibco) supplemented with 10% fetal bovine serum (Thermo Fischer Scientific Inc. Waltham, MA), 10^6 splenocytes or 10^6 bone marrow cells were added to the tPspA-coated plates, followed by incubation for 24 h for bone marrow cells, or five days for spleen cells. Subsequently, the plates were incubated with HRP-conjugated anti-mouse IgA, following the manufacturer's protocol. The resulting spots were visualized using the AEC substrate (Cat: 551951, BD Biosciences, BD, Franklin Lakes, NJ) and quantified utilizing a CTL-Immunospot Analyzer (Cellular Technology, Shaker Heights, OH).

Determination of antibody avidity by ELISA

Determining each experimental group's antibodies' avidity index (AI) was a crucial step in assessing antibody maturation. Microtiter plates (Corning Laboratories, Sigma Aldrich, St. Louis, MO) were coated with the tPspA antigen (2 μg/ml) overnight at 4 °C. After washing three times with distilled water, the plates were incubated with a blocking buffer (PBS containing 0.05% Tween 20 and 0.5% BSA) for 1 h at room temperature. Serially diluted serum in blocking buffer was added to the plates and incubated for 2 h at room temperature. Guanidine hydrochloride (GuHCl) (Cat: 50950, Sigma Aldrich) was added to the blocking buffer to disrupt the low-avidity antibody-antigen complexes. To ensure an optimal range for observing distinctions in avidity among different groups, the GuHCl concentration was titrated within a range of 1.5 to 2.5 M. This observation led to the recognition of 2 M GuHCl as an effective concentration for distinguishing avidity differences. The wells were subjected to three washes, followed by adding 40 μl of a 2 M GuHCl solution in a blocking buffer. The wells were washed three times after a 15-minute incubation at room temperature. The HRP-conjugated anti-mouse IgG secondary antibody (diluted 1:2000) was subsequently added (Table S3). The resulting signal was generated by adding 40 μl of 3,3′,5,5′-tetramethylbenzidine (TMB) substrate (Cat: 555214, BD, Franklin Lakes, NJ), and the reaction was terminated with 40 μl of 1 N H2SO4. The OD_{450} was measured using a microplate reader (Molecular Devices Corp., Menlo Park, CA). For avidity assessment, the AI was employed as a quantitative measure of the average binding strength of IgG antibodies within a serum sample. This AI, a significant indicator, was expressed as a ratio that signifies the proportion of antibodies persistently attached to antigens following treatment with GuHCl. Each serum sample yielded two dilution curves for the series treated with GuHCl (GuHCl +) and untreated (GuHCl$^-$). Endpoint titers corresponding to an OD_{450} of 0.5 were determined. The AI was calculated by dividing the endpoint titer of the serum sample subjected to GuHCl treatment by that of the serum without GuHCl treatment, i.e., AI = titer (GuHCl$^+$) / titer (GuHCl$^-$).

Determination of antigen-specific cytokine production by ELISA

To evaluate antigen-specific cytokine production, we measured IL-4, IL-17, and IFN-γ levels in the culture supernatants of tPspA-stimulated splenocytes. BALB/c mice were intranasally immunized three times with either the FlaB-tPspA fusion protein or FPB NC. Two weeks following the final immunization, splenocytes were isolated from vaccinated mice, and 1×10^6 cells were incubated with 1 μg/mL tPspA antigen for 3 days. Supernatants were then collected, and cytokine concentrations were assayed using commercial ELISA kits (R&D Systems, Minneapolis, MN, USA), specifically the Mouse IFN-γ, Mouse IL-4, and Mouse IL-17 kits. All assays were conducted in accordance with the manufacturer's protocols.

FNR675 conjugation

To evaluate the in vivo biodistribution of FlaB-tPspA or FPB NC, mice were injected in the groin with 60 μg of FNR675-conjugated FlaB-tPspA or 60 μg of FNR675-conjugated FPB NC. To prepare the fluorescence-conjugated proteins, purified FlaB-tPspA or FPB NC was mixed with FNR675-NHS ester (Cat: PWS1515, BioActs, Korea) at 4 °C and stirred overnight. The FNR675-conjugated FlaB-tPspA or FPB NC was then separated from free dye using a centrifugal filter (10 kDa cutoff) (Amicon Ultra®-4, UFC801024), followed by five washes in PBS. The concentration of the conjugated protein was quantified using a calibration curve for the FNR675-NHS ester with a UV-Vis spectrophotometer (UV-2700, Shimadzu, Japan). Three hours post-administration, the inguinal lymph nodes were harvested to assess the micro-biodistribution of FlaB-tPspA or FPB NC using confocal microscopy.

In vivo micro-distribution

To investigate the micro-biodistribution of FPB NC or FlaB-tPspA in lymph nodes, inguinal lymph nodes (iLN) from subcutaneous (S.C.) injections were harvested, embedded in optimal cutting temperature (OCT) compound (Cat: 4583,Sakura) and snap-frozen in liquid nitrogen. Subsequently, seven μm-thick cryosections were prepared. Following cryosectioning, the slides were air-dried for 15 min and blocked for 1 h at room temperature (RT) in PBS containing 0.5% BSA and 0.05% Tween 20. The slides were then incubated for 2 h at RT with biotinylated antibodies at a concentration of 2.5 μg/ml: anti-mouse/human CD45R/B220 (RA3-6B2, Biolegend), anti-mouse CD169 (3D6.112, Biolegend), and anti-mouse CD11c (N418, Biolegend) (Table S3). Biotin-conjugated antibodies were detected using Alexa Fluor 488-conjugated streptavidin (1:200) for 1 h at RT. Images were captured using a confocal microscope (Zeiss LSM-900) and analyzed with ZEN 2012 software (Carl Zeiss).

Germinal center immunofluorescence

To assess germinal center formation in inguinal lymph nodes (iLNs), BALB/c mice were subcutaneously (S.C.) injected with 60 μg of FlaB-tPspA or 60 μg of FPB NC. At week two post-administration, iLNs were harvested and embedded in Tissue-Tek. Additionally, to simulate the intranasal (I.N.) route of administration, mice received I.N. injections of 100 μg of FlaB-tPspA or 100 μg of FPB NC twice with a one-week interval. To mimic the I.N. route of administration, mice were I.N injected with 100 μg of FlaB-tPspA or 100 μg of FPB NC 2 times with 1-week intervals. One week after the final administration, cervical lymph nodes (cLNs) were isolated and embedded in OCT. Subsequently, 7 μm cryostat sections of iLN and cLN were blocked with PBS containing 0.5% BSA and 0.05% Tween 20, followed by staining with a primary antibody cocktail: biotin-conjugated anti-mouse GL7 (GL7, Biolegend), Rat IgG2a anti-mouse B220 (RA3-6B2, Biolegend), and Rabbit IgG anti-mouse CD21/CD35 (EP3093, Abcam). After three washes of 5 min each, the sections were stained with a secondary antibody cocktail: AF647-conjugated streptavidin (405237, Biolegend), AF488 goat anti-rat IgG (A-11006, Invitrogen), AF546 goat anti-rabbit IgG (A-11010, Invitrogen), and BV421-conjugated CD3 (17A2, Biolegend) (Table S3). Images were captured using a Zeiss LSM 900 fluorescence microscope with ZEN 2012 software (Carl Zeiss).

Flow cytometry

The draining iLNs and cLNs were processed into single cells, filtered by 40 μm strainers, and counted the cell numbers. Cells were stained with LIVE/DEAD™ Fixable Near-IR Dead Cell Stain Kit (L34976, Invitrogen). The cells were then washed and blocked with anti-CD16/32 antibody (S17011E, BioLegend) prior to staining with FITC anti-mouse CD11c (N418, Invitrogen), Biotin anti-mouse CD169 (3D6.112, Biolegend), AF488 Streptavidin (405235, Biolegend), BV510 anti-mouse CD45 (30-F11, Biolegend), BV650 anti-mouse CD3 (17A2, Biolegend), BV605 anti-mouse CD4 (GK1.5, Biolegend), PE anti-mouse CD279 (PD-1) (29 F.1A12, Biolegend), Biotin anti-mouse CD185 (CXCR5) (L138D7, Biolegend), PE anti-mouse CD45R/B220 (RA3-6B2, Biolegend), Biotin anti-mouse GL7

(GL7, Biolegend), AF647 Streptavidin (405237, Biolegend) (Table S3). Flow cytometry data were acquired using a CytoFLEX S cytometer (Beckman Coulter) and analyzed with FlowJo software (Tree Star, Ashland, OR).

Statistical analysis

Unless otherwise stated, the results are expressed as the mean ± standard error of the mean (SEM). Statistical difference was analyzed using two-tailed unpaired Student's *t*-tests or one-way ANOVA. The log-rank (Mantel-Cox) test calculated the statistical significance of survival differences. Statistical analyses were performed using the Prism 8.0 software for Windows (GraphPad Software, San Diego, CA). *P* values < 0.05 were considered to indicate statistical significance. The number of subjects used for analyses is indicated in figure legends and that of biological replicates is also disclosed. The statistics correspond to analyses of averaged values in biological replicates, not pooling datasets.

Reporting summary

Further information on research design is available in the Nature Portfolio Reporting Summary linked to this article.

Data availability

All data are included in the Supplementary Information or available from the authors, as are unique reagents used in this article. Source data are provided with this paper.

References

1. Lavelle, E. C. & Ward, R. W. Mucosal vaccines - fortifying the frontiers. *Nat Rev Immunol* **22**, 236–250 (2022).
2. Li, M. et al. Mucosal vaccines: Strategies and challenges. *Immunol Lett* **217**, 116–125 (2020).
3. Kim, S. A. et al. Protein-based nanocages for vaccine development. *J Control Release* **353**, 767–791 (2023).
4. Bhaskar, S. & Lim, S. Engineering protein nanocages as carriers for biomedical applications. *Npg Asia Mater*. **9**, e371 (2017).
5. Lee, E. J., Lee, N. K. & Kim, I. S. Bioengineered protein-based nanocage for drug delivery. *Adv Drug Deliver Rev* **106**, 157–171 (2016).
6. Zhang, B., Tang, G., He, J., Yan, X. & Fan, K. Ferritin nanocage: A promising and designable multi-module platform for constructing dynamic nanoassembly-based drug nanocarrier. *Adv Drug Deliv Rev* **176**, 113892 (2021).
7. Houser, K. V. et al. Safety and immunogenicity of a ferritin nanoparticle H2 influenza vaccine in healthy adults: a phase 1 trial. *Nat Med* **28**, 383–391 (2022).
8. Kanekiyo, M. et al. Self-assembling influenza nanoparticle vaccines elicit broadly neutralizing H1N1 antibodies. *Nature* **499**, 102–106 (2013).
9. Rodrigues, M. Q., Alves, P. M. & Roldao, A. Functionalizing Ferritin Nanoparticles for Vaccine Development. *Pharmaceutics*. **13**, 1621 (2021).
10. Han, J. A. et al. Ferritin protein cage nanoparticles as versatile antigen delivery nanoplatforms for dendritic cell (DC)-based vaccine development. *Nanomed-Nanotechnol* **10**, 561–569 (2014).
11. Yassine, H. M. et al. Hemagglutinin-stem nanoparticles generate heterosubtypic influenza protection. *Nat Med* **21**, 1065–1070 (2015).
12. Samatey, F. A. et al. Structure of the bacterial flagellar protofilament and implications for a switch for supercoiling. *Nature* **410**, 331–337 (2001).
13. Yoon, S. I. et al. Structural basis of TLR5-flagellin recognition and signaling. *Science* **335**, 859–864 (2012).
14. Smith, K. D. et al. Toll-like receptor 5 recognizes a conserved site on flagellin required for protofilament formation and bacterial motility. *Nat Immunol* **4**, 1247–1253 (2003).
15. Zhao, Y. et al. The NLRC4 inflammasome receptors for bacterial flagellin and type III secretion apparatus. *Nature* **477**, 596–600 (2011).
16. Rhee, J. H., Khim, K., Puth, S., Choi, Y. & Lee, S. E. Deimmunization of flagellin adjuvant for clinical application. *Curr Opin Virol* **60**, 101330 (2023).
17. Lowy, J. & McDonough, M. W. Structure of Filaments Produced by Re-Aggregation of Salmonella Flagellin. *Nature* **204**, 125–127 (1964).
18. Cui, B. F. et al. Flagellin as a vaccine adjuvant. *Expert Rev Vaccines* **17**, 335–349 (2018).
19. Lee, S. E. et al. A bacterial flagellin, Vibrio vulnificus FlaB, has a strong mucosal adjuvant activity to induce protective immunity. *Infect Immun* **74**, 694–702 (2006).
20. Hong, S. H. et al. Intranasal administration of a flagellin-adjuvanted inactivated influenza vaccine enhances mucosal immune responses to protect mice against lethal infection. *Vaccine* **30**, 466–474 (2012).
21. Lee, S. E. et al. Flagellin is a strong vaginal adjuvant of a therapeutic vaccine for genital cancer. *Oncoimmunology* **5**, e1081328 (2016).
22. Zheng, J. H. et al. Two-step enhanced cancer immunotherapy with engineered Salmonella typhimurium secreting heterologous flagellin. *Sci Transl Med* **9**, eaak9537 (2017).
23. Puth, S. et al. An all-in-one adjuvanted therapeutic cancer vaccine targeting dendritic cell cytosol induces long-lived tumor suppression through NLRC4 inflammasome activation. *Biomaterials* **286**, 121542 (2022).
24. Nguyen, C. T., Kim, S. Y., Kim, M. S., Lee, S. E. & Rhee, J. H. Intranasal immunization with recombinant PspA fused with a flagellin enhances cross-protective immunity against Streptococcus pneumoniae infection in mice. *Vaccine* **29**, 5731–5739 (2011).
25. Puth, S. et al. A built-in adjuvant-engineered mucosal vaccine against dysbiotic periodontal diseases. *Mucosal Immunol* **12**, 565–579 (2019).
26. Reddington, S. C. & Howarth, M. Secrets of a covalent interaction for biomaterials and biotechnology: SpyTag and SpyCatcher. *Curr Opin Chem Biol* **29**, 94–99 (2015).
27. Keeble, A. H. & Howarth, M. Power to the protein: enhancing and combining activities using the Spy toolbox. *Chem Sci* **11**, 7281–7291 (2020).
28. Zakeri, B. et al. Peptide tag forming a rapid covalent bond to a protein, through engineering a bacterial adhesin. *Proc Natl Acad Sci USA* **109**, E690–E697 (2012).
29. Wang, W. et al. Ferritin nanoparticle-based SpyTag/SpyCatcher-enabled click vaccine for tumor immunotherapy. *Nanomedicine* **16**, 69–78 (2019).
30. Keeble, A. H. et al. Approaching infinite affinity through engineering of peptide-protein interaction. *Proc Natl Acad Sci USA* **116**, 26523–26533 (2019).
31. Li, L., Fierer, J. O., Rapoport, T. A. & Howarth, M. Structural analysis and optimization of the covalent association between SpyCatcher and a peptide Tag. *J Mol Biol* **426**, 309–317 (2014).
32. Wu, X. L., Liu, Y. J., Liu, D., Sun, F. & Zhang, W. B. An Intrinsically Disordered Peptide-Peptide Stapler for Highly Efficient Protein Ligation Both in Vivo and in Vitro. *J Am Chem Soc* **140**, 17474–17483 (2018).
33. Bruun, T. U. J., Andersson, A. M. C., Draper, S. J. & Howarth, M. Engineering a Rugged Nanoscaffold To Enhance Plug-and-Display Vaccination. *Acs Nano* **12**, 8855–8866 (2018).
34. Wang, W. et al. Dual-targeting nanoparticle vaccine elicits a therapeutic antibody response against chronic hepatitis B. *Nat Nanotechnol* **15**, 406–416 (2020).
35. Escolano, A. et al. Immunization expands B cells specific to HIV-1 V3 glycan in mice and macaques. *Nature* **570**, 468–473 (2019).
36. de Benedictis, F. M. et al. Complicated pneumonia in children. *Lancet* **396**, 786–798 (2020).

37. Nunes, M. C. & Madhi, S. A. Review on the immunogenicity and safety of PCV-13 in infants and toddlers. *Expert Rev Vaccines* **10**, 951–980 (2011).
38. Duke, J. A. & Avci, F. Y. Emerging vaccine strategies against the incessant pneumococcal disease. *NPJ Vaccines* **8**, 122 (2023).
39. Avci, F. Y. & Kasper, D. L. How Bacterial Carbohydrates Influence the Adaptive Immune System. *Annu Rev Immunol* **28**, 107–130 (2010).
40. van der Poll, T. & Opal, S. M. Pathogenesis, treatment, and prevention of pneumococcal pneumonia. *Lancet* **374**, 1543–1556 (2009).
41. Avci, F. et al. Glycoconjugates: What It Would Take To Master These Well-Known yet Little-Understood Immunogens for Vaccine Development. *mSphere* **4**, e00520-19 (2019).
42. Elemraid, M. A. et al. Impact of the 7-valent pneumococcal conjugate vaccine on the incidence of childhood pneumonia. *Epidemiol Infect* **141**, 1697–1704 (2013).
43. von Gottberg, A. et al. Effects of vaccination on invasive pneumococcal disease in South Africa. *N Engl J Med* **371**, 1889–1899 (2014).
44. Oliveira, G. S., Oliveira, M. L. S., Miyaji, E. N. & Rodrigues, T. C. Pneumococcal Vaccines: Past Findings, Present Work, and Future Strategies. *Vaccines (Basel)* **9**, 1338 (2021).
45. Pichichero, M. E., Khan, M. N. & Xu, Q. Next generation protein based Streptococcus pneumoniae vaccines. *Hum Vaccin Immunother* **12**, 194–205 (2016).
46. Lane, J. R., Tata, M., Briles, D. E. & Orihuela, C. J. A Jack of All Trades: The Role of Pneumococcal Surface Protein A in the Pathogenesis of Streptococcus pneumoniae. *Front Cell Infect Microbiol* **12**, 826264 (2022).
47. Fukuyama, Y. et al. Nanogel-based pneumococcal surface protein A nasal vaccine induces microRNA-associated Th17 cell responses with neutralizing antibodies against Streptococcus pneumoniae in macaques. *Mucosal Immunol* **8**, 1144–1153 (2015).
48. Kye, Y. C. et al. Intranasal immunization with pneumococcal surface protein A in the presence of nanoparticle forming polysorbitol transporter adjuvant induces protective immunity against the Streptococcus pneumoniae infection. *Acta Biomater* **90**, 362–372 (2019).
49. Jardine, J. et al. Rational HIV immunogen design to target specific germline B cell receptors. *Science* **340**, 711–716 (2013).
50. Tokatlian, T. et al. Innate immune recognition of glycans targets HIV nanoparticle immunogens to germinal centers. *Science* **363**, 649–654 (2019).
51. Hwang, H. S. et al. More robust gut immune responses induced by combining intranasal and sublingual routes for prime-boost immunization. *Hum Vaccin Immunother* **14**, 2194–2202 (2018).
52. Anttila, M., Eskola, J., Ahman, H. & Kayhty, H. Avidity of IgG for Streptococcus pneumoniae type 6B and 23F polysaccharides in infants primed with pneumococcal conjugates and boosted with polysaccharide or conjugate vaccines. *J Infect Dis* **177**, 1614–1621 (1998).
53. Vermont, C. L. et al. Antibody avidity and immunoglobulin G isotype distribution following immunization with a monovalent meningococcal B outer membrane vesicle vaccine. *Infect Immun* **70**, 584–590 (2002).
54. Inoue, T. & Kurosaki, T. Memory B cells. *Nat. Rev. Immunol.* **24**, 5–17 (2023).
55. Zhu, M. Immunological perspectives on spatial and temporal vaccine delivery. *Adv Drug Deliv Rev* **178**, 113966 (2021).
56. Phan, T. G., Green, J. A., Gray, E. E., Xu, Y. & Cyster, J. G. Immune complex relay by subcapsular sinus macrophages and noncognate B cells drives antibody affinity maturation. *Nat Immunol* **10**, 786–793 (2009).
57. Joyce, M. G. et al. SARS-CoV-2 ferritin nanoparticle vaccines elicit broad SARS coronavirus immunogenicity. *bioRxiv*. (2021).
58. Rainho-Tomko, J. N. et al. Immunogenicity and protective efficacy of RSV G central conserved domain vaccine with a prefusion nanoparticle. *NPJ Vaccines* **7**, 74 (2022).
59. Zhou, T. et al. Transplanting supersites of HIV-1 vulnerability. *PLoS One* **9**, e99881 (2014).
60. Ma, X. et al. Nanoparticle Vaccines Based on the Receptor Binding Domain (RBD) and Heptad Repeat (HR) of SARS-CoV-2 Elicit Robust Protective Immune Responses. *Immunity* **53**, 1315–30 e9 (2020).
61. Subramanian, K. et al. Pneumolysin binds to the mannose receptor C type 1 (MRC-1) leading to anti-inflammatory responses and enhanced pneumococcal survival. *Nat Microbiol* **4**, 62–70 (2019).
62. Ercoli, G. et al. Intracellular replication of Streptococcus pneumoniae inside splenic macrophages serves as a reservoir for septicaemia. *Nat Microbiol* **3**, 600–610 (2018).
63. McGeachy, M. J., Cua, D. J. & Gaffen, S. L. The IL-17 Family of Cytokines in Health and Disease. *Immunity* **50**, 892–906 (2019).
64. Lu, Y. J. et al. Interleukin-17A mediates acquired immunity to pneumococcal colonization. *PLoS Pathog* **4**, e1000159 (2008).
65. Ramos-Sevillano, E., Ercoli, G. & Brown, J. S. Mechanisms of Naturally Acquired Immunity to Streptococcus pneumoniae. *Front Immunol* **10**, 358 (2019).
66. Wang, Y. et al. Cross-protective mucosal immunity mediated by memory Th17 cells against Streptococcus pneumoniae lung infection. *Mucosal Immunol* **10**, 250–259 (2017).
67. Moffitt, K. L. et al. T(H)17-based vaccine design for prevention of Streptococcus pneumoniae colonization. *Cell Host Microbe* **9**, 158–165 (2011).
68. Widge, A. T. et al. An influenza hemagglutinin stem nanoparticle vaccine induces cross-group 1 neutralizing antibodies in healthy adults. *Sci Transl Med* **15**, eade4790 (2023).
69. Kelly, H. G. et al. Self-assembling influenza nanoparticle vaccines drive extended germinal center activity and memory B cell maturation. *JCI Insight*. **5**, e136653 (2020).
70. Tatur, J., Hagedoorn, P. L., Overeijnder, M. L. & Hagen, W. R. A highly thermostable ferritin from the hyperthermophilic archaeal anaerobe Pyrococcus furiosus. *Extremophiles* **10**, 139–148 (2006).
71. Hu, L. et al. Physical characterization and formulation development of a recombinant pneumolysoid protein-based pneumococcal vaccine. *J Pharm Sci* **102**, 387–400 (2013).
72. Oliveira, M. L. et al. Combination of pneumococcal surface protein A (PspA) with whole cell pertussis vaccine increases protection against pneumococcal challenge in mice. *PLoS One* **5**, e10863 (2010).
73. Khim, K. et al. Deimmunization of flagellin for repeated administration as a vaccine adjuvant. *NPJ Vaccines* **6**, 116 (2021).

Acknowledgements

The authors thank Myeung Suk Kim, Seol Hee Hong, Yong Jun Bang, Yun Suhk Lee, John Andrews Lavanya Agnes Angalene, Sao Puth, Vandara Loeurng, Jayalakshmi Thiruppathi, Paopachapich Pa and Chheng Y Seng for their excellent assistance with animal experiments and biochemical analyses. This work was supported by the National Research Foundation of Korea (NRF) grant funded by the Korea government (MSIT) (2020R1A5A2031185 to J.H.R.; 2020M3A9G3080282 to L.S.E.; 2019R1A5A2027521 to L.S.E.) and Korea Health Industry Development Institute (KHIDI) RS-2022-KH127978(HV22C0079) to L.S.E.

Author contributions

Conceptualization: J.H.R., S.E.L and T.D.N. Methodology or experiments: T.D.N., H.D.L., G.C.D., K.K. Computational Analysis and 3D Simulation: H.S.J., Y.C. Investigation: J.H.R, S.E.L and T.D.N. Experimental design, analysis and interpretation: J.H.R, S.E.L, T.D.N., H.D.L., G.C.D., Y.K. Funding acquisition: J.H.R. and S.E.L. Supervision: J.H.R. and S.E.L. Writing, review, & editing: J.H.R, S.E.L and T.D.N.

Competing interests
The authors declare no competing interests.

Additional information
Supplementary information The online version contains supplementary material available at https://doi.org/10.1038/s41467-025-58115-8.

Correspondence and requests for materials should be addressed to Shee Eun Lee or Joon Haeng Rhee.

Peer review information *Nature Communications* thanks Dimitri Diavatopoulos, who co-reviewed with Lucille Vanbeek and the other anonymous reviewers for their contribution to the peer review of this work. A peer review file is available.